

**Title:**

Rapid assessment of T-cell receptor specificity of the immune repertoire

**Author(s):**

Xingcheng Lin, Jason T. George, Nicholas P. Schafer, Kevin Ng Chau, Michael E. Birnbaum, Cecilia Clementi, José N. Onuchic & Herbert Levine

Document type: Preprint

Terms of Use: Copyright applies. A non-exclusive, non-transferable and limited right to use is granted. This document is intended solely for personal, non-commercial use.

Citation:

"Xingcheng Lin u.a., 2021, Nature Computational Science volume 1, pages 362–373 (2021) ;
<https://doi.org/10.1038/s43588-021-00076-1>
Archiviert unter <http://dx.doi.org/10.17169/refubium-33989>

Rapid Assessment of T-Cell Receptor Specificity of the Immune Repertoire

Xingcheng Lin^{1,2,3,*}, Jason T. George^{1,4,*}, Nicholas P. Schafer^{1,5}, Kevin Ng Chau⁶,
Michael E. Birnbaum^{7,8,9}, Cecilia Clementi^{1,5,10}, José N. Onuchic^{1,2,5,11,†}, and
Herbert Levine^{1,6,†}

¹Center for Theoretical Biological Physics, Rice University, Houston, TX

²Department of Physics and Astronomy, Rice University, Houston, TX

³Department of Chemistry, Massachusetts Institute of Technology, Cambridge,
MA

⁴Medical Scientist Training Program, Baylor College of Medicine, Houston, TX

⁵Departments of Chemistry, Rice University, Houston, TX

⁶Department of Physics, Northeastern University, Boston, MA

⁷Koch Institute for Integrative Cancer Research, Cambridge, MA

⁸Department of Biological Engineering, Massachusetts Institute of Technology,
Cambridge, MA

⁹Ragon Institute of MIT, MGH, and Harvard, Cambridge, MA

¹⁰Department of Physics, Freie Universität, Berlin, Germany

¹¹Department of Biosciences, Rice University, Houston, TX

*Equal contribution

†To whom correspondence should be addressed: jonuchic@rice.edu,
h.levine@northeastern.edu

22

Abstract

23

24

25

26

27

28

29

30

31

32

33

34

35

Accurate assessment of TCR-antigen specificity at the whole immune repertoire level lies at the heart of improved cancer immunotherapy, but predictive models capable of high-throughput assessment of TCR-peptide pairs are lacking. Recent advances in deep sequencing and crystallography have enriched the data available for studying TCR-p-MHC systems. Here, we introduce a pairwise energy model, RACER, for rapid assessment of TCR-peptide affinity at the immune repertoire level. RACER applies supervised machine learning to efficiently and accurately resolve strong TCR-peptide binding pairs from weak ones. The trained parameters further enable a physical interpretation of interacting patterns encoded in each specific TCR-p-MHC system. When applied to simulate thymic selection of an MHC-restricted T-cell repertoire, RACER accurately estimates recognition rates for tumor-associated neoantigens and foreign peptides, thus demonstrating its utility in helping address the large computational challenge of reliably identifying the properties of tumor antigen-specific T-cells at the level of an individual patient's immune repertoire.

36 **1 Introduction**

37 The advent of new strategies that unleash the host immune system to battle malignant cells represents
38 one of the largest paradigm shifts in treating cancer and has ushered in a new frontier of cancer
39 immunotherapy [1]. Various treatments have emerged, including checkpoint blockade therapy [2,
40 3, 4], tumor antigen vaccine development [5, 6], and the infusion of a donor-derived admixtures of
41 immune cells [7]. A majority of successful treatments to-date rely on the anti-tumor potential of the
42 CD8+ T-cell repertoire, a collection of immune cells capable of differentiating between malignant
43 cells and normal tissue by recognizing tumor-associated neoantigens (TANs) detectable on the cell
44 surface [8]. Therefore, accurately assessing a T-cell repertoire's ability to identify cancer cells by
45 recognizing their tumor antigens lies at the heart of optimizing cancer immunotherapy.

46 A complete understanding of adaptive immune recognition and the tumor-immune interaction
47 has remained a formidable task, owing in part to the daunting complexity of the system. For example,
48 antigens and self-peptides contained in an epitope (i.e. recognizable peptide sequences) space of
49 size $\sim 20^9$ are presented to $\sim 10^7$ unique T-cell clones in each individual [9], a small fraction of
50 the upper limit of TCR diversity ($\sim 10^{20}$) [10, 11]. Moreover, their behavior is tempered via an
51 elaborate thymic negative selection process in order to avoid auto-recognition [12, 13]. Here, T-cell
52 clones, each with uniquely generated T-cell receptors (TCRs), interface with numerous ($\sim 10^4$) self-
53 peptides presented on the major histocompatibility complex (p-MHC) of thymic medullary epithelial
54 cells via TCR CDR3 α and β chains, and survive only if they do not bind too strongly [14, 15, 16].
55 This process, together with systems-level peripheral tolerance [17, 18], imparts T-cells with durable
56 tolerance to major self-peptides and influences many of the recognition properties of the resultant
57 repertoire. The complexity of the adaptive immune system has attracted numerous mathematical
58 modeling efforts quantifying the mechanisms underlying T-cell immune response. Collectively, the
59 field has made significant progress in understanding the population-level effects of tolerance on T-
60 cell recognition and self vs. non-self discrimination [14, 19]. This includes the T-cell repertoire's
61 effectiveness at discerning tumor from self-antigens [20], its ability to impart immunity against
62 current and future threats [21, 22], and the extent of selection pressure that it exerts on an evolving
63 cancer population [23, 24].

64 Any attempt at better understanding these system-scale properties must start with a reliable
65 method to evaluate the interaction between specific TCR-p-MHC pairs. Despite this, a compre-
66 hensive, biophysical model capable of learning the energy contributions of each contact pair in a
67 TCR-p-MHC system and applying them to new predictions remains elusive. To-date, experimental
68 research has integrated solved crystal structures [25, 26] with peptide sequencing [27, 28, 29] to
69 probe the physiochemical hallmarks of epitope-specific TCRs. Publicly available crystal structures
70 have enabled researchers to identify detailed structural features that influence the binding specificity

71 of TCR-p-MHC pairs, and machine learning algorithms have made progress on the complementary
72 task of accurately predicting peptide-MHC binding [30, 31, 32, 33, 34, 35, 36] as well as TCR-
73 peptide binding [37, 38]. However, the limited number of available structures relative to the diver-
74 sity in MHC alleles and TCR-peptide combinations complicates extrapolation to unsolved systems.
75 Alternate template-based structural modeling [39] and docking [40] approaches are limited by cal-
76 culation speeds (at best one structure per minute), thus it is unlikely in the foreseeable future that
77 such strategies can be used to investigate the number of TCR-peptide interactions necessary to study
78 the problem at the immune-repertoire level, as this task easily requires the assessment of more than
79 10^9 pairs simultaneously [16]. Prior attempts have approximated binding affinity by implementing
80 statistical scores calculated from docking algorithms [40]. These scores are trained using examples
81 of generic protein binding and thus lose the unique aspects of the TCR-peptide interactions.

82 To deal with this challenge, we develop a systematic TCR-p-MHC prediction strategy for rapid
83 and accurate assessment of TCR specificity. Our strategy, which we refer to as the Rapid Coarse-
84 grained Epitope TCR (RACER) model, is capable of differentiating between self and foreign anti-
85 gens and can evaluate 10^9 TCR-peptide pairs in the setting of TCR-peptide combinations restricted
86 to a single MHC allele. This method we develop employs supervised machine learning on known
87 TCR-peptide structures and experimental data to derive a coarse-grained, chemically-accurate en-
88 ergy model governing TCR-p-MHC interaction. This strategy was adapted from earlier efforts to
89 predict protein folding [41, 42, 43, 44, 45, 46] and to screen the binding of small molecules [47, 48].
90 The MHC loci, while polymorphic, bind comparable numbers of peptides across various alleles
91 [49]. Our calculations are restricted to a fixed MHC allele, but could be generalized with the use of
92 additional training data. Confining our predictions to TCRs with a given MHC restriction enables
93 the transferability of the method to TCRs that are not included in the training set. The approach
94 provides a tractable means to extract pertinent TCR-peptide interactions so that affinity may be
95 predicted based on similarly restricted TCR-peptide primary sequence data. RACER accurately dis-
96 tinguishes binding peptides across various TCRs and validation tests. Lastly, as a preliminary test of
97 the usefulness of our approach, we simulate thymic selection and show agreement with previously
98 established estimates of T-cell binding energy distributions, tumor neoantigen and foreign peptide
99 recognition rates for a given class of MHC-restricted TCRs [50, 51]. Our *in silico* results share
100 several features observed in experimental data including the degree to which post-selection TCRs
101 preferentially recognize foreign antigen and TANs, in addition to the sequence diversity of epitope-
102 specific TCRs. [52, 28]. Taken together, our results demonstrate RACER's utility in learning the
103 interactions relevant for high-throughput TCR-epitope binding predictions.

104 **2 Results**

105 **2.1 RACER can distinguish peptides that bind strongly to a given TCR from** 106 **those that bind weakly**

107 The RACER optimization protocol (Fig. 1A) utilizes high-throughput deep sequencing data on
108 TCR-peptide interactions across a large peptide library [27], together with known physical con-
109 tacts between TCRs and peptides obtained from deposited crystal structures [53]. The training
110 data comes from cases where all the peptides are displayed by the same allele of the mouse MHC
111 class II molecule. The binding energy between TCRs and peptides, calculated based on a solvent-
112 averaged coarse-grained pairwise model [46], was used as the metric to assess the TCR-peptide
113 binding affinity. The interaction parameters for this solvent-averaged energy model were reopti-
114 mized here specifically for recognizing strong TCR-peptide interactions. Adapting an approach
115 previously implemented for studying folding of proteins [54, 45], the RACER optimization strat-
116 egy trains a pairwise energy model which maximizes TCR-peptide binding specificity. The energy
117 model was optimized by maximizing the Z-score defined to separate the affinities of experimentally
118 determined strong-binding peptides, called “strong binders” hereafter, from computationally gener-
119 ated, randomized decoys¹. The optimized residue type-dependent energy model can then be used
120 to calculate the binding energies of an ensemble of new TCR-peptide systems. As will be shown
121 below, we performed three different levels of test (Fig. 1B), and find the predicted binding ener-
122 gies can differentiate strongly binding peptides from weak ones, provided they are displayed by the
123 same MHC allele as that of the training set. Crucially, accurate predictions can be made even without
124 knowledge of the actual crystal structure, although the predictions are improved when this additional
125 information is available.

126 Fig. 2 summarizes RACER’s predictive performance for a specific TCR (Case I in Fig. 1B).
127 For this fixed TCR, pre-identified strong binding peptides and decoy peptides with randomized se-
128 quences were used to train the energy model (See Methods section for details). Another set of
129 peptides independently verified experimentally as weak binders constitutes the testing set. The re-
130 sulting energy model was then applied to calculate binding energies for the strong binders in the
131 training set as well as the peptides in the testing set. This approach was repeated on three indepen-
132 dent TCRs that are associated with the IE^k MHC-II allele: 2B4, 5CC7 and 226 (Details of these three
133 TCRs are provided in Table S1). Although the experimentally identified weak binders were omitted
134 from the training set, RACER effectively resolves binding energy differences between experimen-
135 tally determined strong and weak binders having Z-scores, calculated in an analogous way as above

¹The Z-score is defined as the difference between the average binding energies of strong binders versus decoys, divided by the standard deviation of the decoy energies. Throughout this manuscript, we report the absolute value of the calculated Z-score, except for Fig. 5C.

136 by replacing decoys with experimentally-determined poor binders, larger than 3.5 in all cases (Fig.
137 2A), thus highlighting the predictive power of this approach.

138 Despite their relative sparsity in antigen space, strong binders play a central role in T-cell epi-
139 tope recognition. It is obviously more difficult to predict strong binders than weak binders. To
140 test RACER's ability to identify strong binders, we performed a leave-one-out cross-validation
141 (LOOCV) test, using data from TCR 2B4 as an example. For each test iteration, one known strong
142 binder was withheld from the training set of 44 strong binders. Our optimization protocol was ap-
143 plied to train the energy model by using the remaining 43 peptides and then predicting the binding
144 energy of the withheld peptide. This prediction was then compared to predicted binding energies of
145 known weak binders, and the procedure was repeated for each of the 44 peptides. Our model is able
146 to accurately distinguish the withheld strong binder in 43 cases (Fig. 2B). This is in stark contrast
147 to a cluster-based attempt at strong binder identification based on peptide sequences alone, which at
148 best correctly identifies 19 out of 44 strong binders (Supplementary note S1). The same LOOCV
149 test was performed for TCR 5cc7 and 226, which correctly identified 120 out of 126 strong binders
150 of 5cc7, and 267 out of 274 strong binders of 226. To further test the limit of RACER in detecting
151 strong binders that have a more diverse sequence coverage, we performed a more demanding set of
152 hold-out tests on a more comprehensive set of data from [27]. RACER can recognize peptides shar-
153 ing little to no sequence identity with the native peptide (Figs. S1, S3), and is still able to recognize
154 strong binders when a substantial portion of the training data is withheld (Supplementary note S2,
155 S3 and Fig. S2, S3).

156 In order to further characterize RACER's predictive power, an independent set of K_d values
157 measured by surface plasmon resonance (SPR) [27] were compared with predicted affinities. The
158 SPR experiments were performed on 9 independent peptide tests for each of the aforementioned
159 three TCRs. RACER was used to predict the binding energies of each of those TCR-peptide pairs,
160 each modeled with the structure of the corresponding TCR as the template. The free energies,
161 $k_B T \log(K_d)$, were compared with calculated binding energies from RACER as a quantitative test
162 of binding affinity prediction accuracy. Lower binding energies indicate stronger binding affinity so
163 that a positive correlation between the $k_B T \log(K_d)$ values and calculated binding energies implies
164 a successful prediction. As shown in Fig. 2C, RACER's prediction of binding affinities for these
165 9 peptides correlates well with experimental measurement, with an average Pearson correlation co-
166 efficient of 0.74. The predicted order of binding affinities is also consistent with those from the
167 experiment, with an average Spearman's rank correlation coefficient of 0.65.

168 **2.2 RACER's residue type-dependent interactions are optimized specifically** 169 **for TCR-peptide recognition**

170 The data utilized by RACER includes strong binders and an input crystal structure, as well as TCR
171 and peptide primary sequences, which determine an interaction pattern that was then used to con-
172 struct a system-specific force field. To illustrate this, we focus on the 2B4 TCR as an example (Fig.
173 3). The crystal structure of TCR 2B4 (Fig. 3A) reveals that there can be many threonine (T) and
174 asparagine (N) residues on the CDR loops region of the TCR. In the strong binder set, these residues
175 tend to interact with specific peptide residues such as alanine (A), as seen for the specific peptide
176 given in the figure. This notion can be formalized by showing the matrix of observed probabilities
177 of close proximity of specific residue pairs. Thus, we see that certain pairs such as A-T and A-N
178 are significantly enriched in the set of strong binders, while much less so in the decoy set (Fig. 3B).
179 This then will mean that the optimized energy model shows the strongest attractions between the
180 A-T, A-N residue pairs (Fig. 3C). This relative enrichment contrasts with the TCR tryptophan (W)
181 residue which frequently interacts with alanine (A) in both strong binders and decoy peptides. As a
182 result, the optimized energy model does not favor the A-W interaction.

183 This energy matrix is rather distinct from those typically used for studying protein folding. In
184 order to compare the RACER-derived interaction matrix to well-established force fields described
185 in the protein folding literature, we substitute for our interaction matrix either the standard AWSEM
186 [46] (optimized on deposited folded proteins) force field or the Miyazawa-Jernigan (MJ) statistical
187 potential [55] (constructed using the probability distribution of contacting residues from deposited
188 proteins) and calculate the corresponding binding energy predictions for the TCR 2B4 peptides. We
189 find that neither of them effectively resolves these groups, with Z-scores of 0.69 and 1.28, respec-
190 tively (Supplementary note 4 and Fig. S4). Similar trends were observed utilizing the peptides
191 corresponding to the 5CC7 and 226 TCRs, demonstrating the necessity of RACER's *de novo* identi-
192 fication of pertinent structural information for studying the TCR-peptide system.

193 **2.3 RACER's interactions enable accurate predictions across various TCRs** 194 **restricted to a given MHC allele**

195 Given RACER's accuracy in resolving test peptides presented to the specific TCR used for training,
196 we next explored the feasibility of extending predictions to additional TCR-peptide pairs albeit with
197 the same MHC restriction. Toward this end, we assessed whether the physical contacts implicitly
198 encoded in RACER's optimized force field were conserved within IE^k-restricted TCR-peptide pairs.
199 The three IE^k-restricted TCRs considered in our analysis all have been tested with peptides bound to
200 the IE^k mouse MHC molecule. The available crystal structures have a significant degree of structural

201 similarity at the TCR CDR3-peptide binding interface (see Fig. 5 of [27]). We further quantified
202 the TCR CDR3-peptide contacts for each pair, constructing a contact map based on their crystal
203 structures (see Methods section for full details). Our results suggest that, despite differences in TCR
204 and peptide primary sequences, the set of strong binding TCR-peptide pairs share common structural
205 features which should aid in imparting transferability of the trained interaction matrix for accurate
206 extrapolation to unknown pairs (Fig. 4). We find however that these features are not preserved across
207 different MHC class II genes (Fig. S5), again indicative of the importance of incorporating structural
208 information.

209 RACER's ability to accurately identify strong binders based on training with a fixed TCR,
210 together with the fact that a majority of the contact structure is preserved within a given MHC-
211 restricted set of TCRs, suggested that we assess RACER's ability to accurately predict binding pep-
212 tides for other similarly restricted TCRs. Toward this end, we apply the energy model optimized
213 using binding data for one of the three TCRs to predict the TCR-peptide binding energies of the
214 remaining two holdout TCRs (Case II in Fig. 1B). To do this, we initially use a known structure
215 for each of the holdouts, and the interaction matrix learned on the training TCR to predict the bind-
216 ing energies of the experimentally determined strong and weak binders for each of those holdout
217 TCRs. Although the Z-scores measured for these alternate TCRs are lower than those found pre-
218 viously in Sec 2.1, RACER still successfully distinguishes a majority of strong binders from weak
219 binders, with an average Z-score of 1.8 (Fig. 5A). This demonstrates that, despite CDR3 primary
220 sequence diversity, distinct TCR-p-MHC systems associated with the same MHC allele still share
221 similar structural-sequence patterns.

222 In order to test whether the incorporation of additional TCR structural information in the op-
223 timization step could improve RACER's predictive accuracy, we next included crystal structures
224 for the remaining TCRs (5cc7 and 226) together with a single strong binder for each case into the
225 training set comprised of 2B4 peptide pairs (See Methods section for details). This procedure was
226 repeated three times by substituting for the training set TCR and peptide pairs. We find that the new
227 energy model demonstrates significant improvement in Z-scores. These results suggest that future
228 incorporation of additional crystal structures of target TCRs may lead to improved resolution of
229 strong and weak binders via refinement of the optimized energy model.

230 To provide an additional test and to quantify our discrimination capability, we used an indepen-
231 dent dataset from [56]. Four independent TCRs (PDB ID: 3QIB, 3QIU, 4P2Q, 4P2R) from their
232 curated benchmark dataset are associated with the IE^k allele; note that three of these overlap with
233 the TCRs in our current study. To test the performance of RACER for different TCR-peptide pairs,
234 we used the energy model trained based on 2B4 (3QIB) to predict the binding energies of both
235 strong and weak binders for the three remaining TCRs. This calculation again uses the structure
236 found for the one strong binding peptide for each of the 3 TCRs. Our calculation re-emphasizes

237 that RACER can successfully distinguish strong binders even when it is trained based on a different
238 TCR (Fig. 5C), with an AUC of 0.89. Of note, when we tested data from the same study involving
239 TCR-p-MHCs with different MHC alleles, RACER cannot pick out strong binders, presumably due
240 to the markedly different TCR-peptide interacting patterns (Fig. S5). As a more comprehensive test
241 of RACER's transferability, we included other TCR-peptide pairs from [56]. RACER is capable of
242 recognizing the strong binders across TCRs with different $V\alpha$ and $V\beta$ genes, and does so more ef-
243 fectively when there are multiple copies of TCR-peptide pairs available for training (Supplementary
244 note S5, Fig. S6).

245 Next we address the question of the extent to which it is necessary to have at hand at least one
246 TCR-p-MHC crystal structure in order to use RACER's interaction matrix to identify other good
247 binders (Case III in Fig. 1B). Of course to evaluate the binding energy we must have a structure; the
248 alternative to having a measured structure for a new sequence is to thread that new CDR3 sequence
249 into the crystal structure used for the training data, which potentially introduces an uncertainty in
250 registration. For the cases at hand, this issue arises only for the α chain as the β chains for all three
251 TCRs are all of length 12 and there is no residual ambiguity. We tested the simplest possible assump-
252 tion, namely that we start at the same place where all three chains have the first two residues AA and
253 leave no gaps. Fig. S8 shows that this procedure again leads to successful discrimination between
254 good and poor binders, with an average Z-score of 2.36. As a comparison, the best performance of
255 a recent sequence-based predictor trained by using artificial neural networks [38] can recognize the
256 strong binders of TCR 5CC7, but not TCR 2B4 and 226 (Supplementary note S6 and Fig. S9). Sim-
257 ilar tests were also performed for the TCR-peptide pairs from [56]. RACER still capably recognize
258 the strong binders across TCRs with different $V\alpha$ and $V\beta$ genes (Supplementary note S5, Fig. S7).
259 Thus, we conclude that the structures are sufficiently similar that not only can we use the interaction
260 matrix derived from a single TCR training set for other TCRs but we can also use the same structure.
261 This then allows us to make estimates at the repertoire scale without the impossible task of creating
262 extremely large numbers of TCR-p-MHC structures.

263 **2.4 RACER-optimized T-cell repertoire binding assessment accurately rep-** 264 **resents thymic selection**

265 Using RACER, we can determine general properties of TCR-p-MHC binding distributions and com-
266 pare to empirical observations. These results highlight the advantage of a method capable of high-
267 throughput analysis. The basic idea follows from the fact shown above that we can make reasonable
268 assessments of binding strength by using only one structure and its associated interaction matrix.
269 Our focus here is the process of negative selection and its effect on the surviving repertoire. Toward
270 this end, we utilized the crystal structure of the 2B4 TCR-peptide contact region to create 10^5 simu-

271 lated TCRs and 10^4 self-peptides by randomizing uniformly the CDR3 and peptide sequences over
272 amino acid space. To avoid registration issues, we always choose simulated TCRs to have exactly
273 the same number of α and β chain residues as does the 2B4 TCR. This was repeated using 10^4 self-
274 peptides and 2000 TCRs, this time weighting the CDR3-peptide interactions by each of the the three
275 contact maps in Fig. 4. The same approach was applied to a model that assumes a strictly diagonal
276 contact map motivated by previous analytical work [20], with randomization of the TCR sequence
277 taken over all possible positions in the contact map.

278 A given TCR survives only if it binds to all self-peptides below a fixed activation threshold. The
279 maximum binding energy over the set of self-peptides for each TCR defines a selection curve (Fig.
280 6A), which describes the percentage of negatively-selected T-cells as a function of the cutoff energy
281 threshold. Selection curves for the three TCR sets using the contact maps in Fig. 4 utilized the
282 RACER energy matrix and compare reasonably to the diagonal contact map motivated by previous
283 analytical work (Fig. 6A red curve). While the variance in each case is similar, mean-shifts in each
284 selection curve correlate directly with the number of contacts in the CDR3 α and β chains (Fig.
285 4). These findings further reinforce the relevance of TCR-p-MHC-specific structural interactions
286 encoded in the RACER-derived energy potential for binding prediction and T-cell repertoire gen-
287 eration. Although empirical estimates of the percentage of surviving TCRs during thymic negative
288 selection vary between 20% and 50% [57, 58, 59], we calculate relevant recognition behavior for all
289 selection rates, restricting our analysis to 50%, when applicable.

290 Most self-peptides present in thymic selection are expected to participate in the deletion of self-
291 reactive T-cells. Previous work has suggested that this desideratum can be used to determine if
292 a high-throughput model is behaving in a statistically sensible manner; specifically, a reasonable
293 model of thymic selection would feature a majority of self-peptides contributing to the selection of
294 immature T-cells. A rank order of these self-peptides based on their ability to recognize unique T-
295 cells, or potency, characterizes the extent to which each self-peptide is utilized in thymic selection.
296 The RACER-derived rank order using the 2B4-optimized data generates reasonable behavior with
297 respect to this criterion (Fig. S10A).

298 One key issue influencing adaptive immune recognition of tumor-associated neoantigens (TANs)
299 is the recognition efficiency of peptides closely related to self (e.g. point mutants) relative to for-
300 eign peptide recognition. The fact that the immune system can in fact be enlisted to attack tumors
301 suggests that negative selection leaves intact the ability to bind strongly to tumor associated anti-
302 gens. Comparison of a post-selection TCR's individual recognition potential shows relatively minor
303 differences between foreign and point-mutant self-peptides (Fig. 6B), with variances of these es-
304 timates overlapping with one another and in line with previous theoretical estimates (Fig. S10B).
305 While individual recognition probability measure a single TCR's ability to recognize antigen, reper-
306 toire recognition probability estimates a particular MHC-restricted post-selection repertoire's ability

307 to recognize antigen. An analogous comparison of the post-selection TCR repertoire recognition
308 probability of foreign and mutant peptides demonstrates that this minimal difference is maintained
309 at the aggregate immune system level (Fig. 6C). This then explains the observed ability of adaptive
310 immune targeting of tumors in a manner that depends on the mutational load of the malignant cells.

311 Our prior theoretical model posited thymic selection as an optimization problem with a sur-
312 vival cutoff near $1/e$ resulting in the production of maximally efficient thymic selection [9, 20].
313 Calculating the product of survival and recognition probabilities yields a broad curve with large
314 values located at intermediate survival cutoffs, including the previously predicted optimal survival
315 cutoff (Fig. S10C). We also can compare our RACER-derived output to immunogenicity scores of
316 experimentally-determined thymic self-peptides, foreign peptides, and TANs [52]. To accomplish
317 this, we calculate the maximal binding energy of post-selection T-cells against each peptide class,
318 a repertoire-level measure of immunogenicity. We find that our model is in broad agreement with
319 other studies [52] that have placed the immunogenicity of TANs intermediary to that of foreign and
320 self-peptides with a distribution closer to the foreign group (Fig. 6D).

321 For additional evaluation of RACER predictions against known experimental findings, we stud-
322 ied the similarity of T-cell CDR3 sequences at the repertoire level generated by RACER-derived
323 TCR-p-MHC specificity maps. These were then compared to the properties of experimentally as-
324 sessed TCR repertoires of known specificity against pre-identified antigens [28]. In our simulation,
325 post-selection TCRs recognizing the top 10 foreign antigens were collected and clustered using a
326 similar discrete Hamming metric that weighted the CDR3 sequences as in [28]. Dendrograms ob-
327 tained from hierarchical clustering identified a diverse set of specific TCRs (Fig. S11A). Because
328 our model only considered a small (10^5) number of TCRs relative to the allowable diversity of CDR3
329 primary sequence space, we then augmented our T-cell repertoire by *in silico* site-directed mutage-
330 nesis to include 100 additional, closely related TCRs for each of the 10 aforementioned peptides,
331 each undergoing identical selection and recognition tests. This augmented list of T-cells accurately
332 recapitulates the empirical observation of a mixed set of specific T-cells, comprised of diverse and
333 homologous clusters of TCR sequences (Fig. S11B), and demonstrates RACER's utility for identi-
334 fying largely diverse TCRs with specificity against a known antigen. Taken together, these results
335 agree with previous studies and reinforce the utility of RACER for performing repertoire-level anal-
336 yses.

3 Discussion

We have introduced RACER, an optimized molecular energy model that can be utilized to quickly assess TCR-peptide interactions and distinguish strong-binding pairs. RACER requires only ~ 0.02 s for evaluating one TCR-peptide pair, thousands of times faster than available alternative approaches, while preserving reasonable prediction accuracy (Figs. 2, 5). Consequently, our method can be used to study large collections of MHC-restricted TCR-peptide pairs, enabling *in silico* studies of thymic selection and prediction of T-cell antigen recognition based on primary sequence data.

3.1 Specificity vs. Generality of the optimized energy model

The unique topology of the TCR-p-MHC structure encodes a system-specific residue-type dependent interaction matrix for TCR-peptide pairs. Significantly, the sequences and structures of TCR-peptide systems were found experimentally to be relatively conserved among various peptides [27, 28, 26]. The preserved sequence and structural features dramatically limit the physiochemical space explorable by TCR-peptide residue pairs. Moreover, since RACER is optimized on a TCR-peptide system, the arrangement of the contacts between TCR and its cognate peptide (Fig. 4) gives rise to a post-optimization energy model (Fig. 3) rather distinct from the traditional hydrophobic-hydrophilic interaction patterns [61] used for studying protein folding, such as the MJ potential [55]. This hypothesis is strongly supported by the observation that RACER is capable of identifying strong binders of corresponding TCRs (Fig. 2) while previous methods fall short (Fig. S4).

The departure of RACER from a typical protein-folding force field also results from the optimization performed for TCR-peptide systems. Because we are interested in resolving strong binders from weak ones with a finite dataset, our optimization distinguishes between these two sets of binders by enlarging their energetic gap in the training process. By maximizing the Z-score between strong and weak binders, RACER learns an effective binding energy which likely amplifies small difference in thermo-stability among candidate binders. Such amplification, however, affects neither the identification of the strong binders of a specific TCR nor the subsequent ensemble study of peptide recognition, since only the order of binding affinities among individual TCR-p-MHC pairs matters for our results.

3.2 Structural information from available crystal structures improves the predictive power of RACER

Our pairwise RACER model offers a novel avenue for developing models that incorporate information contained in available protein structures. Prior investigations have applied artificial neural networks for predicting strong binders of TCR [37, 38] and MHC [30] molecules based only on

369 the primary sequences. Although deep learning can implicitly account for higher-order interactions,
370 such approaches may still be limited by the available sequences that can be identified from exper-
371 iments. RACER alleviates the high demands for primary sequences by including existing crystal
372 structures in a pairwise potential. In order to provide a comprehensive characterization of RACER's
373 predictive power using each of our predictive assessments, our training set was limited to cases that
374 had pre-identified TCR-peptide pairs given their known crystal structure [56]. While RACER effec-
375 tively resolved strong and weak binders in all cases where the training and test peptide were identical,
376 approximately half of test cases derived from this set contained training and test peptides that were
377 dissimilar. In these cases alone, RACER correctly predicts 67% of the examples (Z -score > 1.0).
378 The resulting predictive accuracy demonstrates that our structurally informed pairwise model is able
379 to resolve TCR-p-MHC specificity in a majority of available test cases. Further experimental val-
380 idation will be required to definitively assess RACER's ability to resolve TCR-p-MHC specificity
381 across all possible TCR-peptide pairs within a given MHC allele. This challenge remains a top pri-
382 ority for future investigations on repertoire-level TCR-peptide assessment. In designing RACER to
383 achieve rapid and accurate predictions, our calculation only includes pairwise energetic interactions,
384 while omitting contributions from conformational entropy. While RACER maintains reasonably
385 high predictive accuracy, more accurate assessments of the TCR-p-MHC binding free energy will
386 likely lead to improvements and is a focus of subsequent work.

387 In cases with available crystal structures, contact map analysis revealed a largely conserved in-
388 teraction pattern reproduced across a variety of TCR-peptide pairs associated with the IE^k MHC
389 II allele (Fig. 4), providing an explanation for the transferability of RACER-derived interactions
390 when trained on a particular crystal structure. Moreover, these results contributed to variety in the
391 selection behavior of individual TCRs in that TCR-peptide systems having more interactions in their
392 corresponding contact map were correlated with systematic shifts in their mean binding energies,
393 which subsequently correspond to differences in their post-thymic selection inclusion probability
394 (Fig. 6). Previous investigations have characterized the probability distribution for generating par-
395 ticular TCR sequences in VDJ recombination, and have even suggested that the *a posteriori* observed
396 post-selection TCRs had greater generation probabilities [15, 62], with so-called "public" TCR se-
397 quences being observed in multiple individuals. Incorporation of contact maps into our generative
398 model contributes to variations in T-cell survival probability, and may offer a physical interpretation
399 of why public repertoires may survive thymic selection at higher rates [63], in addition to providing
400 an explicit means of estimating post-selection T-cell prevalence within a given MHC-class restric-
401 tion.

402 **3.3 Recognition of foreign and point-mutated self-peptides**

403 RACER, which leverages structural information to assess binding strength, can be used to simulate
404 the influence of selection on the resulting T-cell repertoire and, hence, on the recognition of TANs
405 across patients and cancer subtypes. Applying our model to CDR₃ α , β chains obtained from T-cell
406 sequencing, together with possible TAN lists generated by deep sequencing of cancer populations
407 could provide a rapid method of generating clinically actionable information for cancer specific
408 TCRs in the form of putative TCR-TAN pairs, provided those TANs are similarly presented on the
409 original MHC [50, 51]. While we focused our analysis on a single MHC restriction, our approach
410 could also be applied to the crystal structure of another TCR-p-MHC pair, together with several
411 known strong and weak binder candidates. More generally, our results also provide credence to the
412 linear constitutive assumption which enables us to sum binding energies of individual residue pairs
413 for quantifying TCR-peptide interactions [20, 14]. Moreover, the predictive accuracy of RACER can
414 be further improved by including additional strong binders from crystal structures that are deposited
415 in the database (Fig. 5B), thus providing a mechanism for additional refinement and improvements
416 in predictive accuracy as more sequence and structural data become available.

417 The relative efficacy of targeting TANs remains an important question with significant clinical
418 implications. We have shown that RACER can readily simulate full-scale thymic selection to pro-
419 duce an MHC-restricted T-cell repertoire. The overall agreement in post-selection behavior between
420 this study and our previous theoretical analysis is reassuring for both approaches, in addition to the
421 general properties of T-cell immunogenicity (Fig. 6D) and recognizing the balance between TCR
422 diversity and similarity observed in experimental data (Fig. S11). Taken together, our findings sug-
423 gest that thymic selection affords little to no recognition protection of peptides closely related to
424 self, thus supporting the notion that T-cells undergoing central tolerance to thymic self-peptides are
425 essentially memorizing a list of antigens to avoid. Given that a large class of TANs are generated
426 via point mutations in self-peptide, this result also provides a quantitative argument for the efficacy
427 of immunotherapies which target point-mutated neoantigens. When compared to experimentally ob-
428 served TCR specificity, the identified antigen-specific T-cells highlights the power of RACER, when
429 assigned a known epitope target, to identify a diverse set of antigen-specific TCRs within high-
430 dimensional TCR primary sequence space. We expect this approach to accelerate therapeutic T-cell
431 discovery by providing a quick and inexpensive screening tool that can then inform more costly
432 confirmatory TCR repertoire sequencing and affinity tests. Currently, we have focused on predicting
433 binding affinities of TCR-peptide pairs restricted to a particular MHC allele, offering a proof-of-
434 principle for epitope identification. This procedure can in general be repeated for other MHC alleles
435 and could be applied to a broad set of clinical scenarios by training on a relatively small number
436 of the most common HLA Class-I alleles, which have been well-studied and have ample available

437 crystal structure data. Toward this end, an immediate future goal will be to generalize RACER for
438 predictions across MHC alleles and gene classes.

439 While important, studying TCR-p-MHC pairwise interactions on the scale of an entire T-cell
440 repertoire is only one factor influencing adaptive immune system recognition. Signaling between
441 other adaptive immune system elements (including helper T-cells and natural killer cells) and intra-
442 cellular factors which influence antigen generation, abundance, and availability on the cell surface
443 also affect recognition rates. Encouraged by the RACER model's reasonable selection and recogni-
444 tion behavior, we propose this optimized framework as the first of its kind tool for tackling general
445 questions regarding the interactions between the T-cell repertoire and relevant antigen landscape. Al-
446 though we calculate static antigen recognition probabilities, the temporal tumor-immune interaction
447 leads to dynamic co-evolution [24] reliant on the quality, abundance, and systems-level signaling of
448 antigens [64]. In the setting of stem cell transplantation approaches, the availability of time series as-
449 sessments of immune cell repertoires, self-peptides, and tumor antigens promises to inform optimal
450 treatment strategies based on the donor immune system and host cancer population.

451 **4 Methods**

452 **4.1 Details of the energy model used in our optimization**

453 To evaluate the binding energies on the basis of a structurally motivated molecular energy model,
454 the framework of a coarse-grained protein energy model, AWSEM force field [46], was utilized for
455 calculating the binding energies between the T-cell receptors (TCRs) and the peptide displayed on
456 top of a MHC molecule. AWSEM is a coarse-grained model with each residue described by the
457 positions of its 3 atoms – $C\alpha$, $C\beta$ and O atoms (except for glycine, which does not have $C\beta$ atoms)
458 [46]. We used the $C\beta$ atom (except for glycine, where the $C\alpha$ atom was used) of each residue to
459 calculate inter-residue interactions. The original AWSEM energy includes both bonded and non-
460 bonded interactions.

$$V_{\text{total}} = V_{\text{bonded}} + V_{\text{nonbonded}} \quad (1)$$

461 Since those residue pairs that contribute to the TCR-peptide binding energy, specifically those from
462 the CDR loops and peptides, are in separate protein chains, only non-bonded interactions are con-
463 sidered. $V_{\text{nonbonded}}$ is composed of three terms:

$$V_{\text{nonbonded}} = V_{\text{pairwise}} + V_{\text{burial}} + V_{\text{database}} \quad (2)$$

464 Among them, V_{burial} is a one-body term describing the propensity of residues to be buried in or
465 exposed on the surface of proteins. V_{database} is a protein sequence-specific term that uses information
466 from existing protein database, such as secondary and tertiary interactions, to ensure locally accurate
467 chemistry of protein structure. Since the TCR-p-MHC system features pairwise interactions between
468 a TCR and its corresponding peptide, only the term V_{pairwise} is used for this study.

469 The pairwise energy of AWSEM potential describes the interactions between any two non-
470 bonded residues and can be further separated into two terms:

$$V_{\text{pairwise}} = V_{\text{direct}} + V_{\text{mediated}} \quad (3)$$

471 V_{direct} captures the direct protein-protein interaction of residues that are in between 4.5 and 6.5 Å.
472 The functional form of V_{direct} is

$$V_{\text{direct}} = \sum_{\substack{i \in \text{TCR} \\ j \in \text{peptide}}} \gamma_{ij}(a_i, a_j) \Theta_{ij}^I \quad (4)$$

473 in which $\Theta_{ij}^I = \frac{1}{4}(1 + \tanh[5.0 \cdot (r_{ij} - r_{\text{min}}^I)])(1 + \tanh[5.0 \cdot (r_{\text{max}}^I - r_{ij})])$ is a switching function
474 capturing the effective range of interactions between two residues (here taken between $r_{\text{min}}^I = 4.5\text{Å}$

475 and $r_{\max}^I = 6.5\text{\AA}$). Thus, two residues are defined to be “in contact” if their distance falls between
476 4.5\AA and 6.5\AA . $\gamma_{ij}(a_i, a_j)$ describes the residue-type dependent interaction strength, and is the
477 most important parameter that enters the optimization of RACER. V_{mediated} describes the longer
478 range interactions of two residues and is not used in this study.

479 **4.2 Optimization of RACER to maximize specificity of TCR-peptide recogni-** 480 **tion**

481 For each interaction type, the $\gamma_{ij}(a_i, a_j)$ parameters constitute a 20-by-20 matrix of parameters that
482 describes the pairwise interaction between any two residues i, j , each with one of the 20 residue
483 types, a_i, a_j . Guided by the principle of minimum frustration [43], $\gamma_{ij}(a_i, a_j)$ was previously op-
484 timized self-consistently to best separate the folded states from the misfolded states of proteins.
485 Distilled into mathematical details, the energy model was optimized to maximize the functional
486 $\delta E/\Delta E$, where δE is the energy gap between folded and misfolded proteins, and ΔE measures the
487 standard deviation of the energies of the misfolded states. An energy model was optimized based on
488 a pool of selected protein structures [65], where a series of decoy structures were generated by either
489 threading the sequences along the existing crystal structures, or by biasing the proteins into molten
490 globule structures using MD simulations [45]. The resultant γ parameter thus determines an energy
491 model that facilitates the folding of proteins with given sequences.

492 Motivated by this idea, RACER was parameterized to maximize the Z-scores for fully sepa-
493 rating TCR strong binders from weak ones. Strong binders were chosen to be those top peptides
494 that survive and were amplified to contain to at least 50 copies after four rounds of experimental
495 deep sequencing processes (details in Section Data used in our analyses) [27], together with the
496 peptides present in the deposited crystal structures [53]. In the experiment of [27], to ensure the
497 correct display of peptides on the MHC, limited diversity was introduced for most distal residues
498 and anchoring residues of peptides. The decoy binder sequences were generated by randomizing
499 the non-anchoring residues of each strong binder thereby generating 1000 copies, and excludes the
500 strong-binder sequences. The γ parameters were then optimized to maximize the stability gap be-
501 tween strong and randomized set of decoy binders, $\delta E = A^T \gamma$, and the standard deviation of decoy
502 energies, $\Delta E^2 = \gamma^T B \gamma$, where the vector A and matrix B are defined as:

$$\begin{aligned} A &= \langle \langle \phi_{\text{direct}} \rangle^{\text{db}} - \phi_{\text{direct}}^{\text{sb}} \rangle \\ B &= \langle \langle \phi_{\text{direct}} \phi_{\text{direct}} \rangle^{\text{db}} - \langle \phi_{\text{direct}} \rangle^{\text{db}} \langle \phi_{\text{direct}} \rangle^{\text{db}} \rangle \end{aligned} \quad (5)$$

503 In the above Eq. 5, “direct” stands for the interaction type, $V_{\text{direct}} \cdot \phi_{\text{direct}}$ is the functional form
504 for $V_{\text{direct}} \cdot \phi_{\text{direct}}$ also summaries the probability of contacts formation (interaction matrix) between

505 pairs of amino acids in a specific TCR-peptide system. The subscripts “db” stands for “decoy
506 binders” and “sb” stands for “strong binders”. The first average is over the 1000 decoy binders
507 generated from one specific strong binder. The second average is over all the strong binders. The
508 maximization of $\delta E/\Delta E = A^T\gamma/\sqrt{\gamma^T B\gamma}$ can be performed effectively by maximizing the func-
509 tional objective $R(\gamma) = A^T\gamma - \lambda_1\Delta$, where $\Delta^2 = \gamma^T B\gamma$. The solution of this optimization gives
510 $\gamma \propto B^{-1}A$. A is a vector containing the difference in the number of interactions of each type in the
511 strong and decoy binders. B is a covariance matrix, which contains information about which types of
512 interactions tend to co-occur in the decoy binders. Finally, γ is a vector that encodes the optimized
513 strengths of the interactions. The dimension of the vector A is (1, 210), that of the matrix B is (210,
514 210), and that of the vector γ is (210, 1). To aid visual presentation, we reshape the γ vector into
515 a symmetric 20 by 20 matrix in Fig. 3C. Finite sampling of decoy binders introduces noise in the
516 optimization process, particularly in B. As such, a filter is applied to reduce the effects of the noise.
517 The filtering scheme was performed by first diagonalizing the B matrix such that $B^{-1} = P\Lambda^{-1}P^{-1}$,
518 where P is composed of the eigenvectors of B and Λ is made up of B’s eigenvalues. The first N modes
519 of B (sorted in descending order by eigenvalue) are retained and the other (210 - N) eigenvalues in
520 Λ are replaced with the Nth eigenvalue of B. The final result is robust to the choice of N. In practice,
521 N is chosen so that no eigenvalue is close to zero. The Wolynes group performed this optimization
522 in an iterative way where the optimized parameters were used for generating a new set of decoy
523 protein structures [66]. In this study, since different peptides are structurally degenerate on top of
524 MHC as observed from experiments [27], only one round of optimization was performed. Since
525 the optimization leaves a scaling factor as a free parameter, throughout this manuscript, the binding
526 energies are presented with reduced units. To obtain binding energies that have physical units, the
527 scaling factor can be further calibrated to fit the experimentally determined binding affinities, such
528 as the K_d values measured by SPR experiments (Fig. 2C).

529 **4.3 Data input used in our analyses**

530 A deep-sequencing technique was developed to assess the binding affinity of a diverse repertoire of
531 MHC-II-presented peptides towards a certain type of TCR [27]. Specifically, 3 types of TCRs: 2B4,
532 5CC7 and 226, were used for selecting peptides upon four rounds of purification. The peptides that
533 survived and enriched with multiple copies bind strongly with the corresponding TCR. In contrast,
534 the peptides present initially but become extinct during purification represent experimentally deter-
535 mined weak binders. For each of the 3 TCRs, the peptides that end up with more than 50 copies
536 after the purification process, together with the peptides presented in the crystal structures, were
537 selected as strong binders. 1000 decoy sequences were generated for each of the strong binders by
538 randomizing the non-anchoring residues. Both strong binders and decoys were included in the train-

539 ing set. In addition, to test the performance of RACER, peptides having at least 8 copies initially but
540 disappearing during purification were selected as experimentally determined weak binders and were
541 assigned to the test set for each TCR. To test the transferability of the model, we used weak-binding
542 peptides of two different TCRs (e.g., 5CC7 and 226) as additional test sets distinct from the TCR
543 used in training (e.g., 2B4).

544 When structural data for a specific TCR-peptide pair of interest is unavailable, we built the
545 structure by homology modeling [67], based on a known TCR-peptide crystal structure incorporating
546 the same TCR. Since potential steric clashes after switching peptide sequences may disfavor the
547 strong binders used in our training set, we used Modeller [67] to refine the structures located at the
548 TCR-peptide interface of strong binders before including them in the training process. Likewise, the
549 binding energies of the experimentally determined weak binders were also evaluated after structural
550 relaxation. The structural relaxation adds several seconds of computational time for each TCR-
551 peptide pair, and thus poses a challenge for large scale repertoire analysis. However, the coarse-
552 grained nature of RACER framework may significantly reduce the probability of side-chain clashes
553 after switching peptide sequences. To test the accuracy of our model prediction without structural
554 relaxation, we calculated the binding energies of strong and weak binders of TCR 2B4 by only
555 switching the peptide sequences, omitting any structural adjustment. Our result (Fig. S12) shows
556 comparable accuracy in separating strong from weak binders, similar to that reported in Fig. 2A. In
557 the same vein, the transferability of RACER was also maintained without structural relaxation (Fig.
558 S8). Encouraged by the accuracy of our coarse-grained model without relaxation, we modeled large
559 pairwise collections of TCR-peptide interactions by only altering their corresponding sequences.

560 For blind assessment of TCR transferability, we ask whether we can improve prediction accuracy
561 if there are available strong binders determined in crystal structures of the target TCRs. To test this,
562 we added interaction matrices calculated from the crystal structures of the other two TCRs as two
563 additional strong binders in the training set. For example, in the case of TCR 2B4, the interaction
564 matrices from the crystal structures of TCR 5CC7 and 226 were added into the training set of TCR
565 2B4, constituting a total of 46 strong binders. The test shows a significant improvement in predicting
566 the binding specificity of TCR 5CC7 and 226 (Fig. 5B).

567 For an additional independent test of the transferability of RACER under the same MHC allele,
568 we used the benchmark set reported in [56]. Four crystal structures are curated in their benchmark
569 set, including three TCRs: 3QIB (2B4), 3QIU (226), 4P2Q (5CC7) and 4P2R (5CC7). Each of them
570 have one strong-binding peptide presented in the crystal structure, and 4 weakly binding peptides.
571 All the TCR-peptide pairs are associated with MHC-II allele IE^k, and three of them overlap with
572 the main dataset reported in [27]. We therefore used the energy model previously trained from TCR
573 2B4 to test its transferability for the other three TCR-peptide pairs. The calculated binding energies
574 were converted into a Z score by referencing to a set of 1000 randomized peptides of corresponding

575 TCRs: $Z = \frac{E_{\text{binding}} - E_{\text{decoys}}}{\sigma(E_{\text{decoys}})}$, with $\sigma(E_{\text{decoys}})$ being the standard deviation of E_{decoys} . The ROC curve
576 and AUC score were calculated by scanning through different thresholds of the Z score. A further
577 test by including more examples from [56] is available at Supplementary note S5, Fig. S6 and S7.

578 **4.4 Accuracy of RACER predictions omitting the crystal structure of target** 579 **TCR-peptide pairs**

580 To test the transferability of RACER without requiring any measured structure for a new TCR, we
581 threaded the sequences of the CDR3 loops of the new TCR on the TCR structure used in our train-
582 ing. The length of CDR3 β chain is the same among three TCRs (2B4: ASSLNWSQDTQY; 5cc7:
583 ASSLNNANSDYT, 226: ASSLNNANSDYT), but the length of CDR3 α chain is different (2B4:
584 AALRATGGNNKLT; 5cc7: AAEASNTNKVV; 226: AAEPSSGQKLV). In order to accommodate
585 such difference when threading the CDR3 α sequences, we used a simple approach: aligning them
586 based on the first two AA residues, leaving two gaps for TCR 5cc7 and 226. Modeller[67] was used
587 to build the new loop structure based on these aligned new sequence, using the single structure in
588 the training set as the template. These homology-modeled structures were then used for calculating
589 the binding energies of the strong and weak binders of the new TCRs, using the trained interaction
590 matrix. We also omitted the step of structural relaxation when replacing a new peptide sequence on
591 the built structure. Such approach is unlikely to reduce RACER's performance, as demonstrated in
592 Fig. S12.

593 **4.5 The leave-one-out cross validation**

594 The Leave-one-out cross validation (LOOCV) was used to test the predictive power of RACER on its
595 ability to identify strong binders. Specifically, one of the 44 strong binders of TCR 2B4 was removed
596 from the training set, and its predicted binding energy E_{pred} was compared with the experimentally
597 determined weak binders. If the median of the weak binders' binding energies is larger than E_{pred}
598 (a larger binding energy is associated with smaller affinity), the testing strong binder is successfully
599 identified. Similar tests were performed for TCR 5cc7 and TCR 226. The performance of RACER is
600 compared with that from the clustering of peptide sequences using the algorithm from CD-Hit [68]
601 (See Supplementary note 1 for details).

602 **4.6 Comparing the correlation of binding energies with the K_d from SPR** 603 **experiments**

604 Surface plasmon resonance (SPR) was performed to assess the binding affinities of the three TCRs
605 towards 9 selected peptides [27]. The correlation between the predicted binding energies from

606 RACER and the dissociation constant K_d evaluated from the SPR experiments thus constitutes a
607 separate set of tests for the accuracy of RACER. We first built a relaxed structure with Modeller [67]
608 for each of those TCR-peptide pairs, using the corresponding TCR structure as the template. We
609 then used the optimized energy model of the corresponding TCR to evaluate the binding energy of
610 each of those TCR-peptide pairs. The K_d values were obtained from fitting the SPR titration curves
611 (Fig. S4F of [27]) using equation $R_{\text{eq}} = \frac{C \cdot R_{\text{max}}}{C + K_d}$ with C , K_d and R_{max} as free parameters. The Pear-
612 son correlation coefficient and the Spearman's rank correlation coefficient between $k_B T \log(K_d)$ and
613 predicted binding energies were used to quantify this correlation.

614 **4.7 Evaluation of contact residues of MHC-restricted TCR-peptide pairs**

615 The contact map of a given TCR-peptide structure was constructed by measuring the proximity W_{ij}
616 between each residue of peptide (residue i) and CDR loops (residue j) based on their mutual distance,
617 using a smoothed step function:

$$W_{ij} = \frac{1 - \tanh(d - d_{\text{max}})}{2}, \quad \text{with } d_{\text{max}} = 6.5 \text{ \AA}. \quad (6)$$

618 Only C_β atoms were included in our calculation (except for glycine, where the C_α atom was
619 used). The CDR3 loops were utilized as defined in the IEDB database [69]. The constructed contact
620 map represents those residues that are spatially close to each other in the given crystal structure.

621 **4.8 Evaluation of different TCR-p-MHC interactions used for statistical study**

622 In order to assess the statistical behavior of the inferential model, we calculated the pairwise binding
623 interactions between a simulated T-cell population of size N_t and collection of $N_n = 10^4$ thymic
624 self-peptides. For this proof-of-principle study, we used TCR 2B4 as an example, uniformly varying
625 the 10^4 amino acids of the peptides, as well as those residues from the TCR that are in spatial
626 contact with the peptide. TCR-peptide pairwise energies were calculated for $N_t = 10^5$ randomized
627 TCR sequences using the RACER energy matrix optimized for TCR 2B4, and $N_t = 2000$ for each
628 of the TCR-p-IE^k systems given in Fig. 4 using energies weighted according to their contact maps,
629 along with a model using a contact map with diagonal interactions (Fig. 6A). Substitution of TCR-
630 peptide sequences with the newly generated ensemble yielded a total of $N_t * N_n$ (10^9 in the 2B4 case;
631 $2 * 10^7$ for each of the cases involving the TCR-p-IE^k and diagonal contact maps) TCR-peptide pairs
632 representing interactions occurring during thymic selection. Given our previous results (Fig. S12),
633 we avoid the computationally expensive task of structural relaxation, and instead calculate pairwise
634 interactions with the original structure, requiring 5,000 CPU hours on an Intel(R) Xeon(R) CPU
635 E5-2650 v2 for the large-scale 2B4-optimized simulation.

636 **4.8.1 Thymic selection**

637 Each T-cell survives if the maximal interaction over all self-peptides does not exceed some up-
638 per threshold. Selection thresholds were chosen to achieve 50% [11]. In all cases, the RACER-
639 optimized energy matrix was used for energy assignment. Thymic selection was performed for each
640 of the TCR-p-IE^k examples and their corresponding contact maps given in Fig. 4 (Fig. 6A). For
641 each TCR-p-IE^k example, $N_t = 2000$ pre-selection TCRs were created by varying uniformly the
642 original TCR CDR3 α and β sequences over amino acid space, keeping the sequence lengths un-
643 changed. A similar randomization yielded $N_n = 10^4$ randomized peptide sequences representing
644 self-peptides. For each of the 2000 randomized TCRs, binding energies were calculated against
645 the 10^4 self-peptides by selecting the corresponding entries in the RACER-optimized energy matrix
646 weighted by the original TCR-p-IE^k contact maps, and the maximum energy was recorded. The
647 fraction of TCRs whose maximal binding energy exceeded the selection threshold E_n traces the
648 survival curves. This procedure, utilizing the RACER-optimized energy matrix, was repeated for a
649 simplified model that utilizes only adjacent contacts (i.e. a strictly diagonal contact map with each
650 entry having weight one) in the TCR-peptide interaction. The number of diagonal elements in the
651 diagonal contact model was taken to be 20 (10 for each of the CDR3 α -peptide and CDR3 β -peptide
652 pairs).

653 **4.8.2 Self-peptide potency**

654 Most self-peptides present in thymic selection are expected to participate in the deletion of self-
655 reactive T-cells. Thus, a reasonable model of thymic selection would feature a majority of self-
656 peptides contributing to the selection of immature T-cells. A rank order of these self-peptides based
657 on their ability to recognize unique T-cells, or potency, characterizes the extent to which each self-
658 peptide is utilized in thymic selection. The rank order of potency was created for the RACER model
659 utilizing the crystal structure of the 2B4 TCR (PDB ID: 3QIB) and its corresponding energy matrix
660 derived from the set of experimentally determined good-binders. The thymic selection process using
661 10^4 self-peptides and 10^5 TCRs for the 2B4-optimized RACER model described above generates a
662 total of 10^9 pairwise binding energies. The negative selection threshold E_n was selected to yield 50%
663 selection, resulting in $\sim 5 \cdot 10^4$ deleted TCRs. The number of TCRs deleted by each self-peptide
664 was recorded. The peptide deleting the most TCRs defines the most potent self-peptide. TCRs
665 recognized by this peptide are removed from the list of total TCRs, and this peptide is similarly
666 removed from the list of self-peptides. This process is repeated on the smaller TCR and self-peptide
667 list to determine the second most potent peptide. Additional iteration until no TCRs remain provides
668 the rank order of self-peptides in decreasing order of potency. The cumulative fraction of deleted
669 relative to total TCRs is plotted in decreasing order of peptide potency.

670 **4.8.3 Antigen recognition probabilities for individual T-cells and T-cell repertoires**

671 Utilizing the same post-selection T-cell repertoire from the previous section, post-selection T-cells
672 were quantified for their ability to recognize random non-self-antigens and tumor neoantigens that
673 differ from one of the N_n thymic self peptides by one residue. 50% selection of TCRs result in
674 approximately $5 \cdot 10^4$ surviving, for which pairwise interactions are generated against 10^3 random
675 and 10^3 point-mutated self-peptides, representing foreign and tumor-associated neoantigens, respec-
676 tively (randomly generated peptides were checked to ensure non-membership in the set of thymic
677 self-peptides). Estimates of individual TCR recognition probability were calculated by averaging
678 the $5 \cdot 10^4$ -by- 10^3 indicator matrix, having values of 1 (resp. 0) corresponding to recognition (resp.
679 no recognition). The previous quantity estimates an individual TCR's antigen recognition ability.
680 Estimates of the corresponding recognition probability for the entire post-selection MHC-restricted
681 T-cell repertoire was calculated by assessing the 1-by- 10^3 vector indicating the presence or absence
682 of at least 1 recognizing TCR. The post-selection individual and repertoire T-cell recognition prob-
683 abilities of random and point-mutant antigens were then compared with previously derived analytic
684 results for two random energy models [20].

685 **5 Acknowledgments**

686 Work at the Center for Theoretical Biological Physics was sponsored by the NSF (Grant PHY-
687 2019745). HL was also support by the NSF (Grant PHY-1935762). JNO was also supported by
688 the NSF (Grant CHE-1614101) and the Welch Foundation (Grant C-1792). JTG was supported by
689 the National Cancer Institute of NIH (F30CA213878). JNO is a CPRIT Scholar in Cancer Research.

690 **6 Data Availability**

691 The data comprised of the peptides recognized by the three TCRs, used for RACER training and
692 testing, are available from [27]. An extended data set of these three TCRs were uploaded at Github:
693 <https://github.com/XingchengLin/RACER.git>. The additional data used for training and testing on
694 different MHC-II TCRs can be found in [56]. All other output from this study are available from the
695 corresponding author upon reasonable request.

696 **7 Code Availability**

697 The full code, along with a demo for predicting TCR-peptide interaction, as well as being applied to a
698 collection of randomly-generated TCRs and peptides, can be found at <https://github.com/XingchengLin/RACER.git>.

References

- 699
- 700 [1] J. Couzin-Frankel, “Cancer Immunotherapy,” Science, vol. 342, pp. 1432–1433, Dec. 2013.
- 701 [2] D. R. Leach, M. F. Krummel, and J. P. Allison, “Enhancement of antitumor immunity by
702 CTLA-4 blockade,” Science (New York, N.Y.), vol. 271, pp. 1734–1736, Mar. 1996.
- 703 [3] H. O. Alsaab, S. Sau, R. Alzhrani, K. Tatiparti, K. Bhise, S. K. Kashaw, and A. K. Iyer,
704 “PD-1 and PD-L1 Checkpoint Signaling Inhibition for Cancer Immunotherapy: Mechanism,
705 Combinations, and Clinical Outcome,” Frontiers in Pharmacology, vol. 8, p. 561, 2017.
- 706 [4] M. Sadelain, I. Rivière, and S. Riddell, “Therapeutic T cell engineering,” Nature, vol. 545,
707 no. 7655, pp. 423–431, 2017.
- 708 [5] P. A. Ott, Z. Hu, D. B. Keskin, S. A. Shukla, J. Sun, D. J. Bozym, W. Zhang, A. Luoma,
709 A. Giobbie-Hurder, L. Peter, C. Chen, O. Olive, T. A. Carter, S. Li, D. J. Lieb, T. Eisenhaure,
710 E. Gjini, J. Stevens, W. J. Lane, I. Javeri, K. Nellaippan, A. M. Salazar, H. Daley, M. Sea-
711 man, E. I. Buchbinder, C. H. Yoon, M. Harden, N. Lennon, S. Gabriel, S. J. Rodig, D. H.
712 Barouch, J. C. Aster, G. Getz, K. Wucherpfennig, D. Neuberg, J. Ritz, E. S. Lander, E. F.
713 Fritsch, N. Hacohen, and C. J. Wu, “An immunogenic personal neoantigen vaccine for patients
714 with melanoma,” Nature, vol. 547, no. 7662, pp. 217–221, 2017.
- 715 [6] P. Johansen, T. Storni, L. Rettig, Z. Qiu, A. Der-Sarkissian, K. A. Smith, V. Manolova, K. S.
716 Lang, G. Senti, B. Müllhaupt, T. Gerlach, R. F. Speck, A. Bot, and T. M. Kündig, “Antigen
717 kinetics determines immune reactivity,” Proceedings of the National Academy of Sciences,
718 vol. 105, pp. 5189–5194, Apr. 2008.
- 719 [7] J. J. Molldrem, K. Komanduri, and E. Wieder, “Overexpressed differentiation antigens as tar-
720 gets of graft-versus-leukemia reactions,” Current Opinion in Hematology, vol. 9, pp. 503–508,
721 Nov. 2002.
- 722 [8] A. K. Abbas, A. K. Abbas, A. H. Lichtman, and S. Pillai, Cellular and molecular immunology.
723 2018.
- 724 [9] R. J. De Boer and A. S. Perelson, “How diverse should the immune system be?,” Proceedings.
725 Biological Sciences, vol. 252, pp. 171–175, June 1993.
- 726 [10] V. I. Zarnitsyna, B. D. Evavold, L. N. Schoettle, J. N. Blattman, and R. Antia, “Estimating the
727 diversity, completeness, and cross-reactivity of the T cell repertoire,” Frontiers in Immunology,
728 vol. 4, p. 485, Dec. 2013.

- 729 [11] A. J. Yates, “Theories and Quantification of Thymic Selection,” Frontiers in Immunology,
730 vol. 5, 2014.
- 731 [12] H. von Boehmer, “Thymic selection: a matter of life and death,” Immunology Today, vol. 13,
732 pp. 454–458, Nov. 1992.
- 733 [13] G. J. Nossal, “Negative selection of lymphocytes,” Cell, vol. 76, pp. 229–239, Jan. 1994.
- 734 [14] A. Kosmrlj, A. K. Jha, E. S. Huseby, M. Kardar, and A. K. Chakraborty, “How the thymus de-
735 signs antigen-specific and self-tolerant T cell receptor sequences,” Proceedings of the National
736 Academy of Sciences, vol. 105, pp. 16671–16676, Oct. 2008.
- 737 [15] Y. Elhanati, A. Murugan, C. G. Callan, T. Mora, and A. M. Walczak, “Quantifying selection in
738 immune receptor repertoires,” Proceedings of the National Academy of Sciences of the United
739 States of America, vol. 111, pp. 9875–9880, July 2014.
- 740 [16] J. Ishizuka, K. Grebe, E. Shenderov, B. Peters, Q. Chen, Y. Peng, L. Wang, T. Dong, V. Pas-
741 quetto, C. Oseroff, and others, “Quantitating T cell cross-reactivity for unrelated peptide anti-
742 gens,” The Journal of Immunology, vol. 183, no. 7, pp. 4337–4345, 2009. Publisher: Am
743 Assoc Immunol.
- 744 [17] M. M. Davis, “Not-So-Negative Selection,” Immunity, vol. 43, pp. 833–835, Nov. 2015.
- 745 [18] C. F. Arias, M. A. Herrero, J. A. Cuesta, F. J. Acosta, and C. Fernández-Arias, “The growth
746 threshold conjecture: a theoretical framework for understanding T-cell tolerance,” Royal
747 Society Open Science, vol. 2, p. 150016, July 2015.
- 748 [19] V. Detours, R. Mehr, and A. S. Perelson, “A quantitative theory of affinity-driven t cell reper-
749 toire selection,” Journal of theoretical biology, vol. 200, no. 4, pp. 389–403, 1999.
- 750 [20] J. T. George, D. A. Kessler, and H. Levine, “Effects of thymic selection on T cell recognition
751 of foreign and tumor antigenic peptides,” Proceedings of the National Academy of Sciences of
752 the United States of America, vol. 114, no. 38, pp. E7875–E7881, 2017.
- 753 [21] A. Mayer, V. Balasubramanian, A. M. Walczak, and T. Mora, “How a well-adapting immune
754 system remembers,” Proceedings of the National Academy of Sciences, vol. 116, pp. 8815–
755 8823, Apr. 2019.
- 756 [22] G. Altan-Bonnet, T. Mora, and A. M. Walczak, “Quantitative immunology for physicists,”
757 Physics Reports, 2020. Publisher: Elsevier.

- 758 [23] J. T. George and H. Levine, “Stochastic modeling of tumor progression and immune evasion,”
759 Journal of Theoretical Biology, vol. 458, pp. 148–155, 2018.
- 760 [24] J. T. George and H. Levine, “Sustained coevolution in a stochastic model of cancer–immune
761 interaction,” Cancer Research, vol. 80, no. 4, pp. 811–819, 2020.
- 762 [25] T. P. Riley, L. M. Hellman, M. H. Gee, J. L. Mendoza, J. A. Alonso, K. C. Foley, M. I.
763 Nishimura, C. W. Vander Kooi, K. C. Garcia, and B. M. Baker, “T cell receptor cross-reactivity
764 expanded by dramatic peptide–MHC adaptability,” Nature Chemical Biology, vol. 14, pp. 934–
765 942, Oct. 2018.
- 766 [26] N. K. Singh, T. P. Riley, S. C. B. Baker, T. Borrmann, Z. Weng, and B. M. Baker, “Emerging
767 Concepts in TCR Specificity: Rationalizing and (Maybe) Predicting Outcomes,” Journal of
768 Immunology (Baltimore, Md.: 1950), vol. 199, no. 7, pp. 2203–2213, 2017.
- 769 [27] M. E. Birnbaum, J. L. Mendoza, D. K. Sethi, S. Dong, J. Glanville, J. Dobbins, E. Özkan, M. M.
770 Davis, K. W. Wucherpfennig, and K. C. Garcia, “Deconstructing the Peptide-MHC Specificity
771 of T Cell Recognition,” Cell, vol. 157, pp. 1073–1087, May 2014.
- 772 [28] P. Dash, A. J. Fiore-Gartland, T. Hertz, G. C. Wang, S. Sharma, A. Souquette, J. C. Crawford,
773 E. B. Clemens, T. H. O. Nguyen, K. Kedzierska, N. L. La Gruta, P. Bradley, and P. G. Thomas,
774 “Quantifiable predictive features define epitope-specific T cell receptor repertoires,” Nature,
775 vol. 547, no. 7661, pp. 89–93, 2017.
- 776 [29] T. Kula, M. H. Dezfoulian, C. I. Wang, N. S. Abdelfattah, Z. C. Hartman, K. W. Wucherpfennig,
777 H. K. Lyerly, and S. J. Elledge, “T-scan: a genome-wide method for the systematic discovery
778 of t cell epitopes,” Cell, vol. 178, no. 4, pp. 1016–1028, 2019.
- 779 [30] M. Nielsen, C. Lundegaard, P. Worning, S. L. Lauemøller, K. Lamberth, S. Buus, S. Brunak,
780 and O. Lund, “Reliable prediction of T-cell epitopes using neural networks with novel sequence
781 representations,” Protein Science, vol. 12, pp. 1007–1017, May 2003.
- 782 [31] M. Andreatta and M. Nielsen, “Gapped sequence alignment using artificial neural networks:
783 application to the MHC class I system,” Bioinformatics, vol. 32, pp. 511–517, Feb. 2016.
- 784 [32] V. Jurtz, S. Paul, M. Andreatta, P. Marcatili, B. Peters, and M. Nielsen, “NetMHCpan-4.0:
785 Improved Peptide–MHC Class I Interaction Predictions Integrating Eluted Ligand and Peptide
786 Binding Affinity Data,” The Journal of Immunology, vol. 199, pp. 3360–3368, Nov. 2017.
- 787 [33] B. Reynisson, B. Alvarez, S. Paul, B. Peters, and M. Nielsen, “NetMHCpan-4.1 and
788 NetMHCIIpan-4.0: improved predictions of MHC antigen presentation by concurrent motif

- 789 deconvolution and integration of MS MHC eluted ligand data,” Nucleic Acids Res., vol. 48,
790 pp. W449–W454, July 2020.
- 791 [34] J. R. Abella, D. A. Antunes, C. Clementi, and L. E. Kavraki, “Ape-gen: A fast method for
792 generating ensembles of bound peptide-mhc conformations,” Molecules, vol. 24, no. 5, p. 881,
793 2019.
- 794 [35] J. R. Abella, D. A. Antunes, C. Clementi, and L. E. Kavraki, “Large-scale structure-based pre-
795 diction of stable peptide binding to class i hla using random forests,” Frontiers in Immunology,
796 vol. 11, p. 1583, 2020.
- 797 [36] B. Chen, M. S. Khodadoust, N. Olsson, L. E. Wagar, E. Fast, C. L. Liu, Y. Muftuoglu,
798 B. J. Sworder, M. Diehn, R. Levy, M. M. Davis, J. E. Elias, R. B. Altman, and A. A. Al-
799 izadeh, “Predicting HLA class II antigen presentation through integrated deep learning,” Nature
800 Biotechnology, vol. 37, pp. 1332–1343, Nov. 2019.
- 801 [37] V. I. Jurtz, L. E. Jessen, A. K. Bentzen, M. C. Jespersen, S. Mahajan, R. Vita, K. K. Jensen,
802 P. Marcatili, S. R. Hadrup, B. Peters, and M. Nielsen, “NetTCR: sequence-based prediction of
803 TCR binding to peptide-MHC complexes using convolutional neural networks,” bioRxiv, Oct.
804 2018.
- 805 [38] I. Springer, H. Besser, N. Tickotsky-Moskovitz, S. Dvorkin, and Y. Louzoun, “Prediction of
806 Specific TCR-Peptide Binding From Large Dictionaries of TCR-Peptide Pairs,” Frontiers in
807 Immunology, vol. 11, Aug. 2020.
- 808 [39] R. Gowthaman and B. G. Pierce, “TCRmodel: high resolution modeling of T cell receptors
809 from sequence,” Nucleic Acids Research, vol. 46, pp. W396–W401, July 2018.
- 810 [40] B. G. Pierce and Z. Weng, “A flexible docking approach for prediction of T cell receptor-
811 peptide-MHC complexes,” Protein Science: A Publication of the Protein Society, vol. 22,
812 pp. 35–46, Jan. 2013.
- 813 [41] C. Clementi, H. Nymeyer, and J. N. Onuchic, “Topological and energetic factors: what deter-
814 mines the structural details of the transition state ensemble and “en-route” intermediates for
815 protein folding? an investigation for small globular proteins,” Journal of Molecular Biology,
816 vol. 298, pp. 937–953, May 2000.
- 817 [42] J. Wang and G. M. Verkhivker, “Energy Landscape Theory, Funnels, Specificity, and Optimal
818 Criterion of Biomolecular Binding,” Physical Review Letters, vol. 90, May 2003.

- 819 [43] J. D. Bryngelson and P. G. Wolynes, “Spin glasses and the statistical mechanics of protein
820 folding,” Proceedings of the National Academy of Sciences, vol. 84, pp. 7524–7528, Nov.
821 1987.
- 822 [44] V. I. Abkevich, A. M. Gutin, and E. I. Shakhnovich, “Improved design of stable and fast-folding
823 model proteins,” Folding and Design, vol. 1, no. 3, pp. 221–230, 1996.
- 824 [45] N. P. Schafer, B. L. Kim, W. Zheng, and P. G. Wolynes, “Learning To Fold Proteins Using
825 Energy Landscape Theory,” Israel Journal of Chemistry, vol. 54, pp. 1311–1337, Aug. 2014.
- 826 [46] A. Davtyan, N. P. Schafer, W. Zheng, C. Clementi, P. G. Wolynes, and G. A. Papoian,
827 “AWSEM-MD: Protein Structure Prediction Using Coarse-Grained Physical Potentials and
828 Bioinformatically Based Local Structure Biasing,” The Journal of Physical Chemistry B,
829 vol. 116, pp. 8494–8503, July 2012.
- 830 [47] J. Wang, X. Zheng, Y. Yang, D. Drueckhammer, W. Yang, G. Verkhivker, and E. Wang, “Quan-
831 tifying intrinsic specificity: a potential complement to affinity in drug screening,” Phys Rev
832 Lett, vol. 99, p. 198101, Nov. 2007.
- 833 [48] Z. Yan, X. Zheng, E. Wang, and J. Wang, “Thermodynamic and kinetic specificities of ligand
834 binding,” Chemical Science, vol. 4, no. 6, p. 2387, 2013.
- 835 [49] X. Rao, R. J. De Boer, D. van Baarle, M. Maiers, and C. Kesmir, “Complementarity of bind-
836 ing motifs is a general property of hla-a and hla-b molecules and does not seem to effect hla
837 haplotype composition,” Frontiers in immunology, vol. 4, p. 374, 2013.
- 838 [50] E. Alspach, D. M. Lussier, A. P. Miceli, I. Kizhvatov, M. DuPage, A. M. Luoma, W. Meng,
839 C. F. Lichti, E. Esaulova, A. N. Vomund, et al., “Mhc-ii neoantigens shape tumour immunity
840 and response to immunotherapy,” Nature, vol. 574, no. 7780, pp. 696–701, 2019.
- 841 [51] J. C. Castle, S. Kreiter, J. Diekmann, M. Löwer, N. Van de Roemer, J. de Graaf, A. Selmi,
842 M. Diken, S. Boegel, C. Paret, et al., “Exploiting the mutanome for tumor vaccination,” Cancer
843 research, vol. 72, no. 5, pp. 1081–1091, 2012.
- 844 [52] M. Ogishi and H. Yotsuyanagi, “Quantitative Prediction of the Landscape of T Cell Epitope
845 Immunogenicity in Sequence Space,” Frontiers in Immunology, vol. 10, Apr. 2019.
- 846 [53] E. W. Newell, L. K. Ely, A. C. Kruse, P. A. Reay, S. N. Rodriguez, A. E. Lin, M. S. Kuhns,
847 K. C. Garcia, and M. M. Davis, “Structural Basis of Specificity and Cross-Reactivity in T
848 Cell Receptors Specific for Cytochrome *c* –I-E ^k,” The Journal of Immunology, vol. 186,
849 pp. 5823–5832, May 2011.

- 850 [54] R. A. Goldstein, Z. A. Luthey-Schulten, and P. G. Wolynes, “Protein tertiary structure recog-
851 nition using optimized Hamiltonians with local interactions,” Proceedings of the National
852 Academy of Sciences, vol. 89, pp. 9029–9033, Oct. 1992.
- 853 [55] S. Miyazawa and R. L. Jernigan, “Estimation of effective interresidue contact energies from
854 protein crystal structures: quasi-chemical approximation,” Macromolecules, vol. 18, pp. 534–
855 552, May 1985.
- 856 [56] E. Lanzarotti, P. Marcatili, and M. Nielsen, “Identification of the cognate peptide-mhc target
857 of t cell receptors using molecular modeling and force field scoring,” Molecular immunology,
858 vol. 94, pp. 91–97, 2018.
- 859 [57] C. Sinclair, I. Bains, A. J. Yates, and B. Seddon, “Asymmetric thymocyte death underlies the
860 CD4:CD8 T-cell ratio in the adaptive immune system,” Proceedings of the National Academy
861 of Sciences, vol. 110, pp. E2905–E2914, July 2013.
- 862 [58] L. Ignatowicz, W. Rees, R. Pacholczyk, H. Ignatowicz, E. Kushnir, J. Kappler, and P. Marrack,
863 “T cells can be activated by peptides that are unrelated in sequence to their selecting peptide,”
864 Immunity, vol. 7, pp. 179–186, Aug. 1997.
- 865 [59] J. Zerrahn, W. Held, and D. H. Raulet, “The MHC reactivity of the T cell repertoire prior to
866 positive and negative selection,” Cell, vol. 88, pp. 627–636, Mar. 1997.
- 867 [60] W. Humphrey, A. Dalke, and K. Schulten, “VMD: Visual molecular dynamics,” Journal of
868 Molecular Graphics, vol. 14, pp. 33–38, Feb. 1996.
- 869 [61] L. H. Kapcha and P. J. Rossky, “A Simple Atomic-Level Hydrophobicity Scale Reveals Protein
870 Interfacial Structure,” Journal of Molecular Biology, vol. 426, pp. 484–498, Jan. 2014.
- 871 [62] P. G. Thomas and J. C. Crawford, “Selected before selection: a case for inherent antigen bias in
872 the t-cell receptor repertoire,” Current Opinion in Systems Biology, vol. 18, pp. 36–43, 2019.
- 873 [63] A. Madi, E. Shifrut, S. Reich-Zeliger, H. Gal, K. Best, W. Ndifon, B. Chain, I. R. Cohen, and
874 N. Friedman, “T-cell receptor repertoires share a restricted set of public and abundant cdr3
875 sequences that are associated with self-related immunity,” Genome research, vol. 24, no. 10,
876 pp. 1603–1612, 2014.
- 877 [64] J. T. George and H. Levine, “Implications of tumor–immune coevolution on cancer evasion and
878 optimized immunotherapy,” Trends in Cancer, vol. 7, no. 4, pp. 373–383, 2021.

- 879 [65] G. A. Papoian, J. Ulander, M. P. Eastwood, Z. Luthey-Schulten, and P. G. Wolynes, “From
880 The Cover: Water in protein structure prediction,” Proceedings of the National Academy of
881 Sciences, vol. 101, pp. 3352–3357, Mar. 2004.
- 882 [66] K. K. Koretke, Z. Luthey-Schulten, and P. G. Wolynes, “Self-consistently optimized energy
883 functions for protein structure prediction by molecular dynamics,” Proceedings of the National
884 Academy of Sciences, vol. 95, pp. 2932–2937, Mar. 1998.
- 885 [67] B. Webb and A. Sali, “Comparative Protein Structure Modeling Using MODELLER,” Current
886 Protocols in Bioinformatics, vol. 54, June 2016.
- 887 [68] L. Fu, B. Niu, Z. Zhu, S. Wu, and W. Li, “CD-HIT: accelerated for clustering the next-
888 generation sequencing data,” Bioinformatics, vol. 28, pp. 3150–3152, Dec. 2012.
- 889 [69] R. Vita, J. A. Overton, J. A. Greenbaum, J. Ponomarenko, J. D. Clark, J. R. Cantrell, D. K.
890 Wheeler, J. L. Gabbard, D. Hix, A. Sette, and B. Peters, “The immune epitope database (IEDB)
891 3.0,” Nucleic Acids Res., vol. 43, pp. D405–412, Jan. 2015.

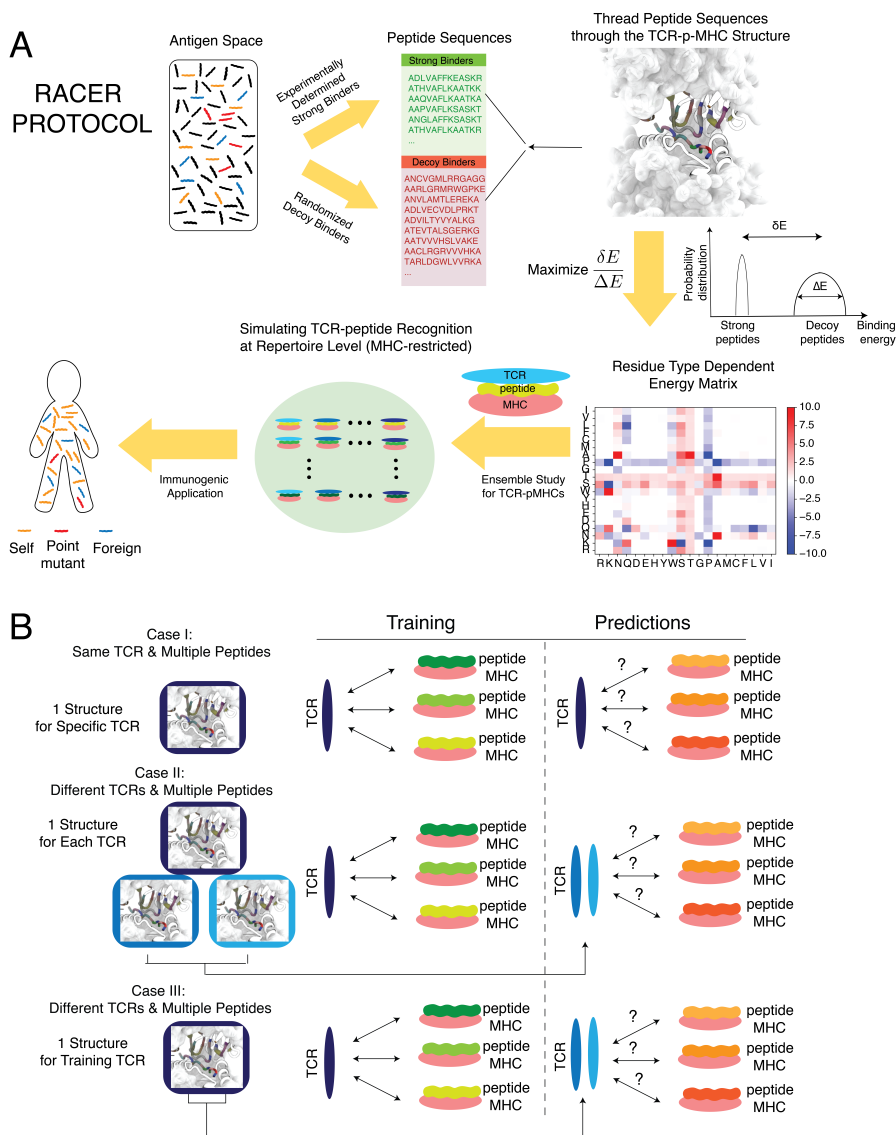


Figure 1: Summary of the modeling approach employed in this study. **A.** The optimization of RACER starts from a series of TCR binders obtained from the deep-sequencing experiments [27], as well as the corresponding TCR-p-MHC crystal structures deposited in the database [53]. The sequences of the strong binders, as well as the generated decoy binders from randomizing the non-anchoring sequences of the strong binders, are collected for parameterizing a pairwise energy model which maximizes the energetic gap between the strong binders and a randomized set of decoys. The resulting energy model can be used to quickly evaluate the binding affinities of an ensemble of TCR-peptide interactions at the population level. The calculated binding affinities can be used for simulating the negative selection process in the thymus, as well as measuring the recognition probability of the post-selection TCRs. Finally, this kind of ensemble study can be used for immunogenic applications that require input from an entire T-cell repertoire. **B.** Three tests were conducted to evaluate the performance of RACER. Case I: the training set includes one TCR-p-MHC structure and multiple peptide sequences. The test set includes the same TCR structure and a separate set of peptide sequences. Case II: the training set includes one TCR-p-MHC structure and multiple peptide sequences. The test set includes two different TCR structures (restricted on the same MHC allele) and two separate sets of peptide sequences. Structures for the two additional test TCRs are included in predictions. Case III: The training set includes one TCR-p-MHC structure and multiple peptide sequences. The test set includes only the sequences of two different TCRs (restricted on the same MHC allele) and two separate sets of peptides. Only the structure from the original training TCR was used in prediction (The interactions of interest are indicated by double-sided arrows between TCR and p-MHC).

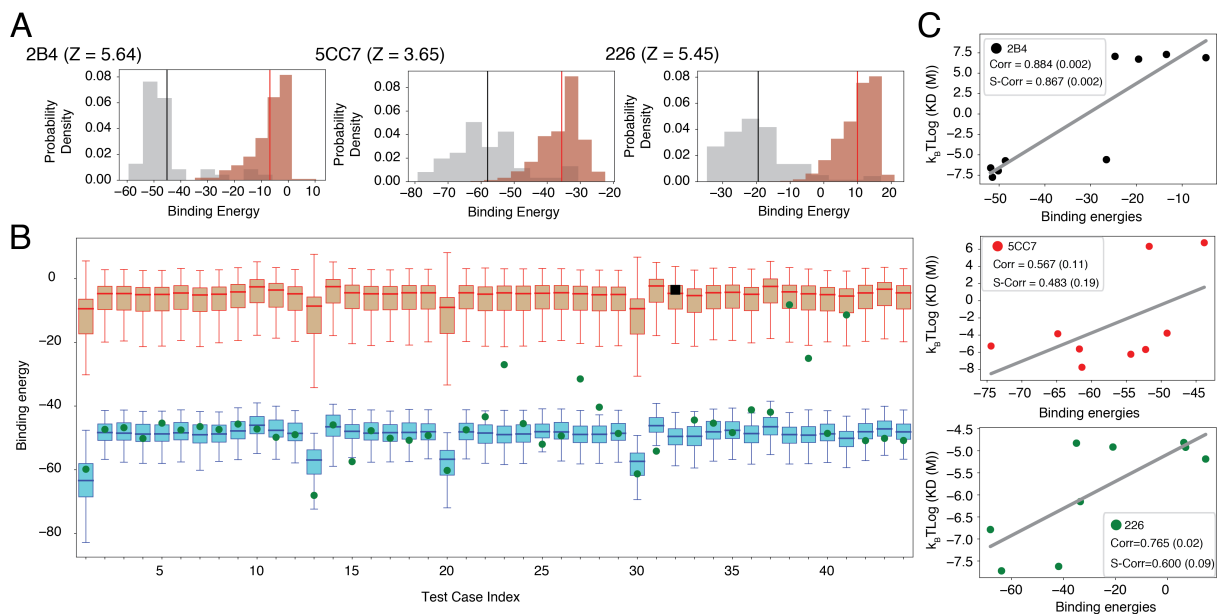


Figure 2: RACER can fully separate the strong binders of a specific TCR from its weak binders. **A.** For three TCRs (2B4, 5CC7 and 226) whose strong and weak binders have been experimentally determined [27], the RACER-derived calculated binding energies can well separate strong binders from weak ones of each individual TCR. **B.** In the leave-one-out-cross-validation exemplified using TCR 2B4, RACER can successfully recognize the withheld strong binders in 43 out of 44 tests, where the predicted binding energies of the withheld test binder (green) is lower than the median (red bar) of the experimentally determined weak binders. The only exception is marked as a black square. The whiskers are placed at the first and last datum points that fall within (m, M), where $m = Q1 - 1.5IQR$ and $M = Q3 + 1.5IQR$, $IQR = Q3 - Q1$ represents the interquartile range. **C.** In a completely independent testing data measured by surface plasmon resonance (SPR) [27], the calculated binding energies of testing peptides correlate well with their experimentally determined dissociation constant K_d . Best-fit linear regression is depicted for each case. Corr: Pearson correlation coefficient. S-Corr: Spearman's rank correlation coefficient. The p-value of each correlation coefficient is reported in the parenthesis.

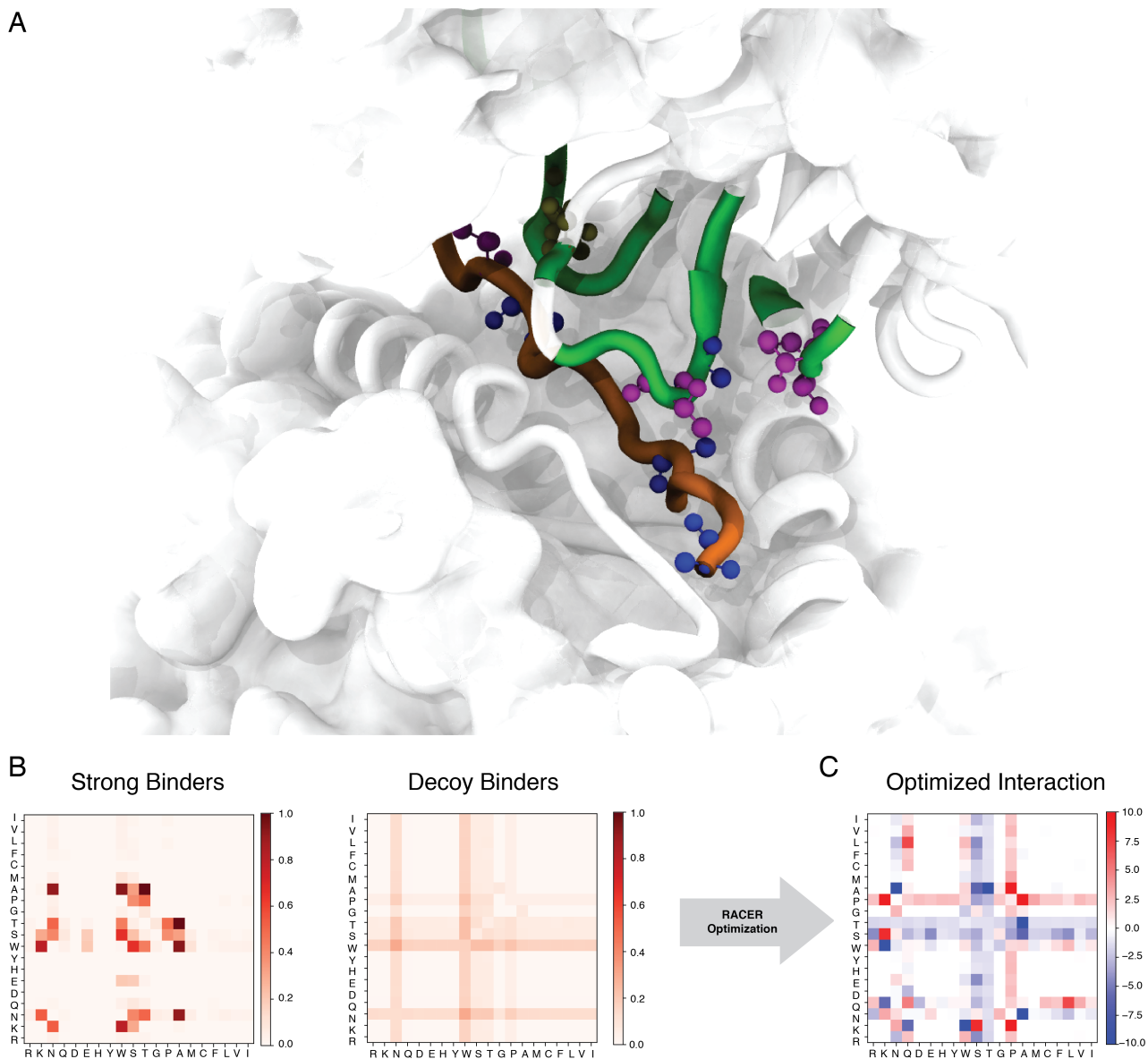


Figure 3: The specific contact pattern from the TCR-peptide structures dictates a optimized energy model different from those of a typical protein-folding force field. **A**. The 3D crystal structure of the 2B4 TCR bound to a specific peptide (PDBID: 3QIB). The parts of the structure that are in contact between the TCR and peptide are color-highlighted as green (TCR) and orange (peptide). Also shown are residues alanine (blue), threonine (magenta) and asparagine (tan) which are prevalent in this structure (CPK representation [60]). **B**. The probability of contact formation between each two of the 20 amino acids in the set of strong binders (left) and the set of randomized decoy binders (right) of TCR 2B4. **C**. The residue-based interaction strength determined by RACER for TCR 2B4. A more negative value indicates a stronger attractive interaction between the corresponding two residues.

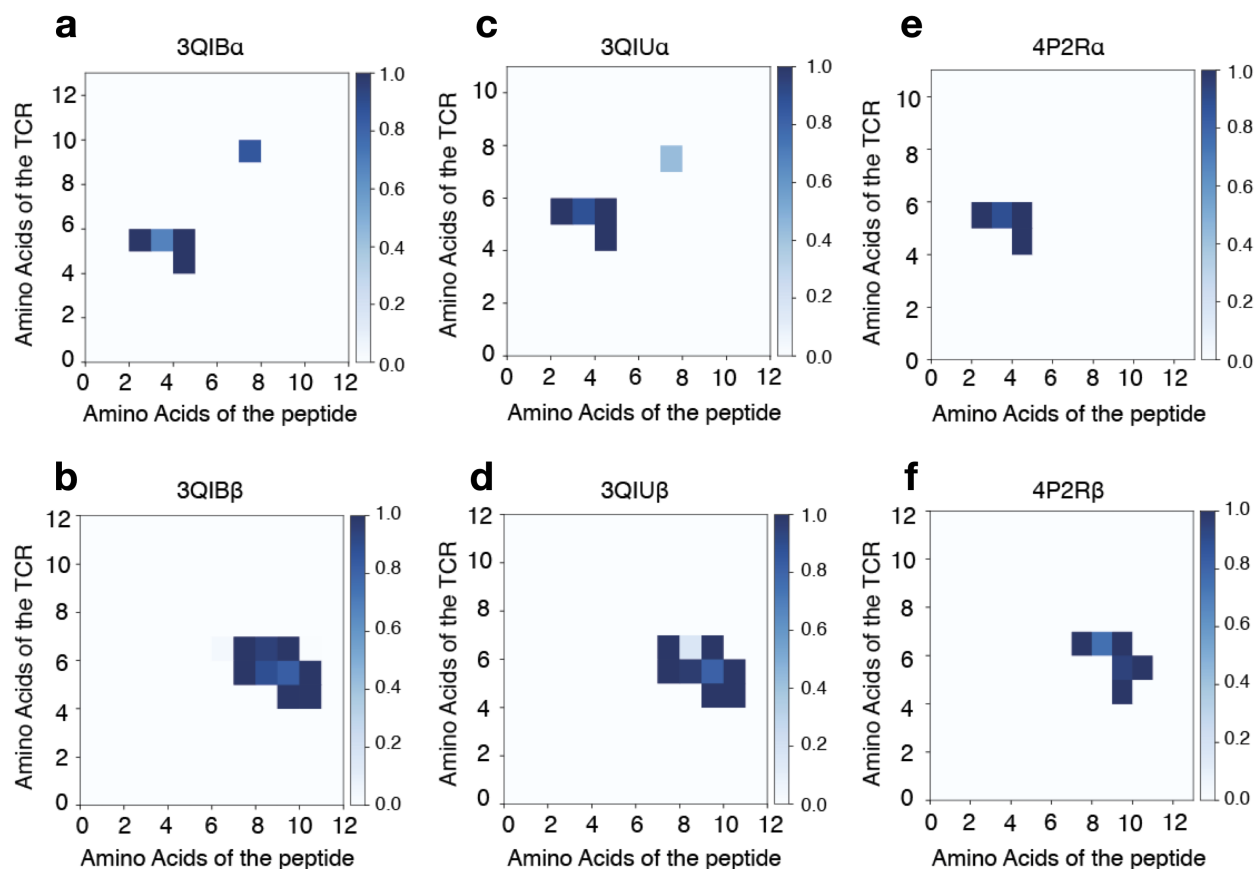


Figure 4: The contact maps of TCR-peptide pairs within the same MHCII allele share structural similarity. Contact maps are calculated using distances from each pairwise TCR-peptide amino acid combination using Eq. 6 for the following MHC-II IE^k-restricted TCR-peptide pairs: 3QIB - peptide ADLIAYLKQATK with TCR 2B4 **A.** CDR3 α (AALRATGGNNKLT) and **B.** CDR3 β (ASSLNWSQDTQY) chains; 3QIU - peptide ADLIAYLKQATK with TCR 226 **C.** CDR3 α (AAEPSSGQKLV) and **D.** CDR3 β (ASSLNNANSDYT) chains; 4P2R - peptide ADGVAFLLTPFKA with TCR 5c7 **E.** CDR3 α (AAEASNTNKVV) and **F.** CDR3 β (ASSLNNANSDYT) chains. Similarity in interaction topology across TCR-peptide pairs is observed by comparing the contact silhouette of interacting coordinates for the α (top row) and β (bottom row) TCR sequences.

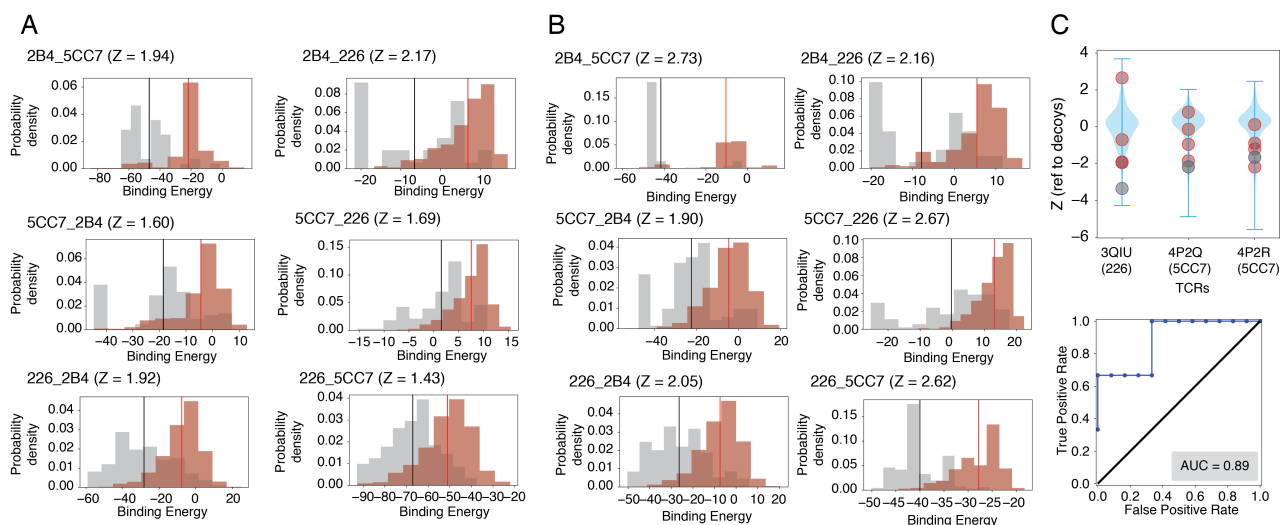


Figure 5: RACER shows transferability in terms of predicting TCR-p-MHC interactions across different TCRs. **A.** The energy model trained based on one TCR (e.g. 2B4) is capable of resolving the experimentally determined strong binders from weak binders of the other two TCRs (e.g., 5CC7 and 226). **B.** By adding strong binders from crystal structures of the other two TCRs into training sets, RACER can be further improved for identifying the experimentally determined strong binders. The title of each figures follows the format of “target_training TCRs”, e.g., “2B4_5CC7” means using the energy model trained from TCR 5CC7 for predicting the peptide binding affinities of TCR 2B4. “Xtals” means the strong binders from the crystal structures of the other two TCRs were added into the training set. **C.** Upper panel: The energy model trained on TCR 2B4 is used to predict the binding energies of sequences from other TCRs associated with the IEk-associated TCRs [56]. Z-scores of known strong binders (grey) and weak binders (orange) provided by [56] were calculated referenced to a set of 1000 decoy peptides with randomized sequences (blue violin plot), with lower Z-scores indicating better predictive performance. Lower panel: The calculated Z-scores of each TCR were used to depict Corresponding ROC curve and AU-ROC (0.89, lower panel).

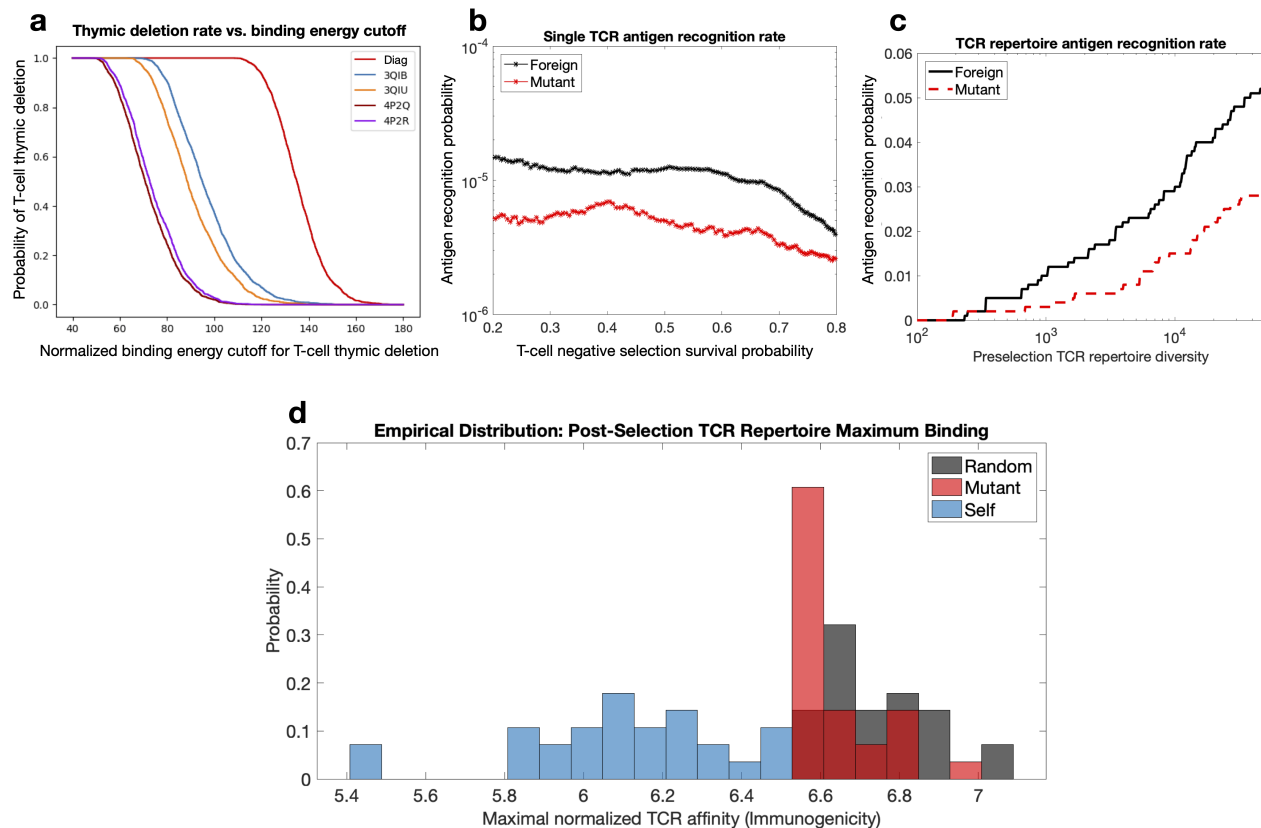


Figure 6: T-cell repertoire simulations of thymic selection and antigen recognition in the RACER model. RACER-derived simulations of TCR recognition exhibit sensible thymic selection and similarity in the recognition rates of foreign and point-mutated self antigens. **A.** Simulated thymic selection curves (T-cell recognition probability as a function of negative selection binding energy cutoff) incorporating the effects of non-adjacent contacts (given in Fig. 4) using $N_n = 10^4$ uniformly randomized self-peptides and $N_t = 2000$ randomized IE^k -restricted TCRs. 4P2Q and 4P2R (purple) use T-cells generated by randomizing the CDR3 region of TCR 5cc7, while 3QIB (blue) randomizes the CDR3 of TCR 2B4, and 3QIU (yellow) randomizes the CDR3 of TCR 226 (in all cases, randomized CDR3 lengths were unchanged from the original TCR) (red curve uses RACER energy using a diagonal contact map model whose study here is motivated by previous work [20]). **B.** Utilizing RACER-derived energy assessments from the 2B4 crystal structure, the probability of recognizing foreign and point-mutant antigens for individual post-selection T-cells is plotted as a function of the percentage of TCRs surviving negative selection (ordinate of the graph in panel a, simulations averaged over all post-selection TCRs with pairwise interactions amongst 10^3 random peptides and 10^3 point-mutant peptides). **C.** The recognition probability of foreign (black) and mutant (red) peptides by the entirety of the TCR repertoire is plotted as a function of pre-selection TCR repertoire diversity, with negative selection thresholds giving 50% survival. **D.** RACER-derived immunogenicity of foreign, mutant, and self antigen. The maximum binding affinity over all post-selection T-cells for immunogenic random (gray) and point-mutated self-peptides (red) is compared to that of thymic self-peptides (green) (There were 28 point-mutated peptides that had at least one T-cell recognition event. To keep an equal number of peptides in each distribution, we compared these with the top 28 similarly ordered foreign peptides and 28 randomly chosen self-peptide groups).